Structural and Spectroscopic Characterization of Iron(III) Dioxoporphodimethene Complexes and Their Autoreduction to an Iron(II) Complex in Pyridine

Alan L. Balch,* Bruce C. Noll, Marilyn M. Olmstead, and Shane L. Phillips

Department of Chemistry, University of California, Davis, California 95616

Received April 17, 1996[⊗]

Three iron complexes of the *meso*-dioxo derivative of octaethylporphryin (*trans*-H_2OEPO_2) were characterized by X-ray diffraction. Green $ClFe^{III}$(*trans*-$OEPO_2$)·$1.5C_6H_6$ crystallizes in the monoclinic space group $P2_1/c$ with $a = 13.766(3)$ Å, $b = 19.075(3)$ Å, $c = 15.217(3)$ Å, $\beta = 99.87(2)°$ at 123 K with $Z = 4$. Refinement of 2712 reflections with $F > 6.0\sigma(F)$ and 223 parameters yielded $R = 0.0624$, $R_w = 0.0596$. The iron complex contains a domed dioxoporphodimethene macrocyclic ligand. The observation of a five-coordinate iron(III) ion with an axial Fe−Cl distance of 2.232(2) Å and in-plane Fe−N distances averaging 2.082 Å is consistent with its high-spin ($S = {}^5/_2$) character. This monomer is readily converted to the green {Fe^{III}(*trans*-$OEPO_2$)}$_2$O using aqueous hydroxide. {Fe^{III}(*trans*-$OEPO_2$)}$_2$O crystallizes in the monoclinic space group $C2/c$ with $a = 23.541(8)$ Å, $b = 15.392(5)$ Å, $c = 18.686(8)$ Å, and $\beta = 90.09(3)°$ at 294 K with $Z = 8$. Refinement of 3472 reflections with $F > 6.0\sigma(F)$ and 393 parameters yielded $R = 0.0484$, $R_w = 0.0527$. The complex possesses a crystallographically imposed 2-fold symmetry axis that passes through the oxo ligand. The dioxoporphodimethene ligands within the molecule are roof-shaped and fold away from each other. The axial Fe−O distance is 1.749(1) Å with longer in-plane Fe−N distances (average 2.077 Å). The Fe−O−Fe angle of 165.4(2)° deviates significantly from linearity and is more acute than related porphyrin complexes. Pyridine solutions of either the iron(III) monomer or μ-oxo dimer autoreduce over a period of days to give $(py)_2Fe^{II}$(*trans*-$OEPO_2$). This red compound crystallizes in the space group $P2_1$ with $a = 19.177(4)$ Å, $b = 20.039(4)$ Å, $c = 10.547(2)$ Å, and $\beta = 100.36(3)°$ at 130 K with $Z = 2$. Refinement of 5090 reflections with one restraint and 984 parameters yielded R1 = 0.0684, wR2 = 0.1763. The complex crystallizes with two distinct molecules in the asymmetric unit; each molecule contains a different degree of disorder with respect to the *trans* meso oxygen atoms (50/50, 71/29). Each independent molecule exhibits severe ruffling of the macrocycle. The six coordinate iron(II) center is diamagnetic. The axial Fe−N(pyridine) distances average 1.98 Å, and the in-plane Fe−N(pyrrole) distances average 1.95 Å. A common trend observed for the dioxoporphodimethene macrocycle in all of these structures is an elongation toward the *trans* oxidized meso carbons. These complexes were originally prepared as *cis* and *trans* isomeric mixtures that can be enriched in the *trans* isomer by fractional crystallization. This is evident in their distinctive ^{1}H NMR spectra. In addition, these compounds are characterized by electron impact mass spectrometry and UV−visible, ESR, and infrared spectroscopies.

Introduction

Metalloporphyrins are subject to oxidative degradation which limits their utility as catalysts but which also facilitates their catabolism.[1] It is widely believed that the initial stage of heme oxidative degradation results in the incorporation of an oxygen atom (or hydroxyl group) at a meso position of the porphyrin.[2] A likely intermediate of this sort, $(py)_2Fe^{III}(OEPO^{\bullet})$, **1**, has recently been isolated and structurally characterized.[3] Upon exposure to dioxygen in pyridine solution, complex **1** undergoes transformation into verdoheme, **2**,[4−6] and the iron biliverdin complex **3**[7] (Scheme 1, eq 1). In contrast, when Ni^{II}(OEPOH), **4,** is exposed to dioxygen in pyridine solution, the relatively stable free radical complex **5,** $(py)_2Ni^{II}(OEPO^{\bullet})$, is formed.[8] With further exposure to air, **5** is gradually transformed into a mixture of the *trans*- and *cis*-dioxoporphyrin complexes, **6** and **7** (Scheme 1, eq 2).[8,9] Thus the central metal ion plays a crucial role in directing the further oxidation of the porphyrin periphery. In order to facilitate the identification of iron complexes that are likely to form during heme degradation processes, we have undertaken the preparation and characterization of the iron

[⊗] Abstract published in *Advance ACS Abstracts,* October 1, 1996.

(1) (a) O'Carra, P. In *Porphyrins and Metalloporphyrins*; Smith, K. M., Ed.; Elsevier: New York, 1975; p 123. (b) Schmid, R.; McDonagh, A. F. In *The Porphyrins*; Dolphin, D., Ed.; Academic Press: New York, 1979; Vol. 6, p 258. (c) Brown, S. B. In *Bilirubin*; Heirwegh, K. P. M., Brown, S. B., Eds.; CRC Press, Inc.: Boca Raton, FL, 1982; Vol. 2, p 1. (d) Bissell, D. M. In *Liver: Normal Function and Disease. Bile Pigments and Jaundice*; Ostrow, J. D., Ed.; Marcel Dekker, Inc.: New York, 1986; Vol. 4, p 133. (e) Maines, M. D. *Heme Oxygenase: Clinical Applications anf Functions*; CRC Press: Boca Raton, FL, 1992. (f) Chang, C. K.; Avilés, G.; Bag, N. *J. Am. Chem. Soc.* **1994**, *116*, 12127.
(2) Bonnett, R.; Dimsdale, M. J. *J. Chem. Soc., Perkin Trans.* **1972**, *79*, 2540.
(3) Balch, A. L.; Koerner, R.; Latos-Grażyński, L.; Noll, B. C. *J. Am. Chem. Soc.* **1996**, *118*, 2760.
(4) Lagarias, J. C. *Biochem. Biophys. Acta* **1982**, *717*, 12.
(5) Balch, A. L.; Latos-Grażyński, L.; Noll, B. C.; Olmstead, M. M.; Szterenberg, L., Safari, N. *J. Am. Chem. Soc.* **1993**, *115*, 1422.
(6) Balch, A. L.; Koerner, R.; Olmstead, M. M. *J. Chem. Soc., Chem. Commun.* **1995**, 873.
(7) Balch, A. L.; Latos-Grażyński, L.; Noll, B. C.; Olmstead, M. M.; Safari, N. *J. Am. Chem. Soc.* **1993**, *115*, 9056.
(8) Balch, A. L.; Noll, B. C.; Phillips, S. L.; Reid, S. M.; Zovinka, E. P. *Inorg. Chem.* **1993**, *32*, 4730.
(9) Balch, A. L., Olmstead, M. M., Phillips, S. L. *Inorg. Chem.* **1993**, *32*, 3931.

S0020-1669(96)00423-5 CCC: $12.00

Scheme 1

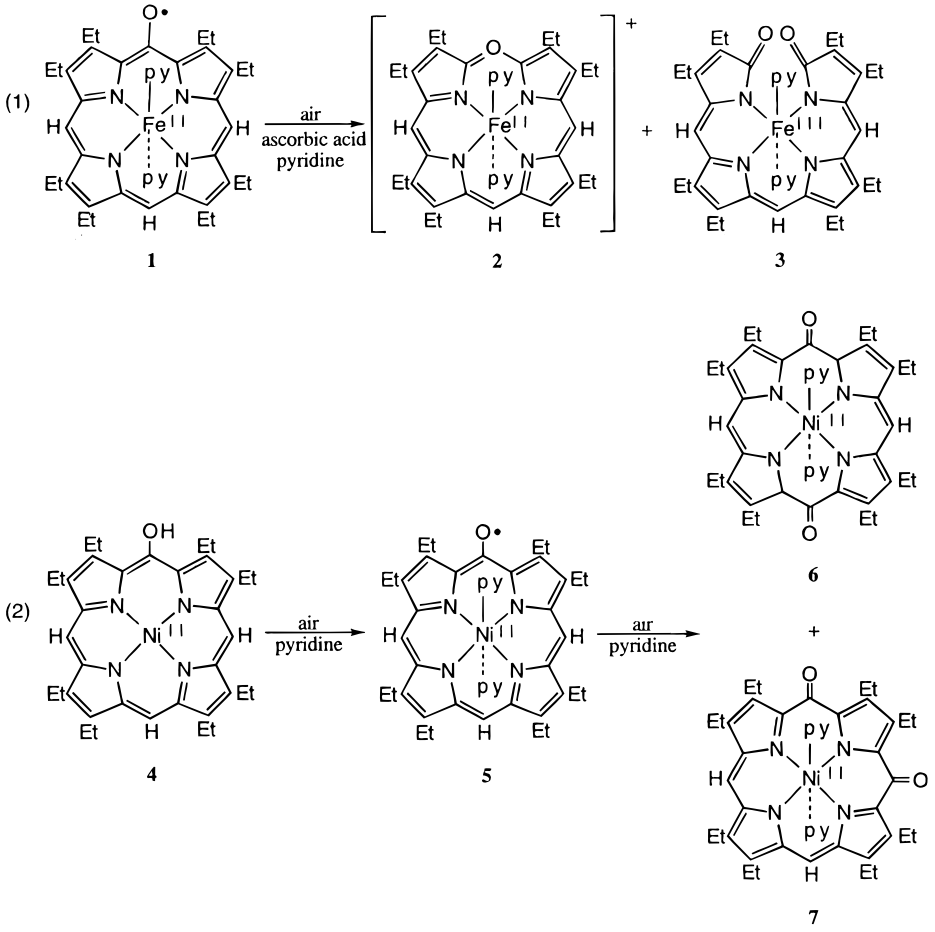

complexes of the meso-dioxo derivatives of octaethylporphyrin: **8**, *trans*-H_2OEPO_2, and **9**, *cis*-H_2OEPO_2. These two ligands

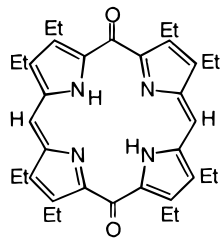

8, (*trans*-H_2OEPO_2)

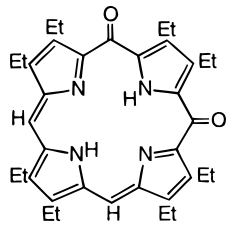

9, (*cis*-H_2OEPO_2)

are readily obtained by the oxidation of zinc(II)octaethylporphyrin with thallium(III) trifluoroacetate.[9−12] The isomeric free bases are obtained in a 4:1 ratio of **8**:**9**. The free bases themselves have so far eluded attempts at separation, but the nickel complexes, **6** and **7**, have been separated by column chromatography.[9]

Results

Formation and Spectroscopic Characterization of Monomeric Iron(III) Complexes. Metallation of an isomeric mixture of the dioxo free bases **8** and **9** was achieved by addition of iron(II) bromide hexahydrate to a slowly boiling brown solution of the ligands in tetrahydrofuran. The green insertion products were recovered from a dichloromethane solution and washed with hydrobromic acid to give a mixture (4:1 *trans*:*cis*) of $BrFe^{III}(OEPO_2)$, **10a**, and **11a**. Washing with hydrochloric acid afforded the chloro compounds, **10b** and **11b**. The two isomers did not separate during chromatography, and fractional crystallization was only reasonably efficient in producing a sample for X-ray diffraction.

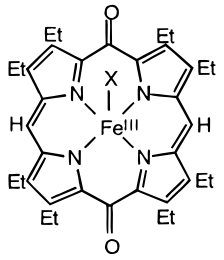

10, XFe^{III}(*trans*-$OEPO_2$)
a, X = Br; **b**, X = Cl

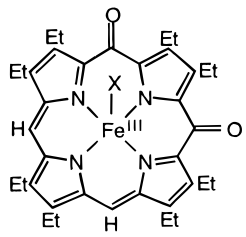

11, XFe^{III}(*cis*-$OEPO_2$)
a, X = Br; **b**, X = Cl

Clear evidence that two isomeric complexes are present in the metallated samples is given by their NMR spectra. The ^1H NMR spectrum of the bromide isomers, **10a** and **11a**, in chloroform solution is shown in Figure 1. The paramagnetism of these compounds is clearly demonstrated by the large downfield shifts of the meso and methylene resonances. The patterns of resonances for **10a** and **11a** are consistent with their idealized symmetry of C_{2v} and C_s respectively. The methylene protons of each ethyl group are diastereotopic since there is axial coordination on only one side of the porphyrin plane. The less symmetric **11a** has eight downfield methylene resonances labeled **11** in Figure 1, while complex **10a** exhibits only four downfield methylene resonances marked **10**. The expansions

(10) Barnett, G. H.; Hudson, M. F.; McCombie, S. W.; Smith, K. M. *J. Chem. Soc., Perkin Trans.* **1973**, 691.
(11) Barnett, G. H.; Evans, B.; Smith, K. M. *Tetrahedron* **1975**, *31*, 2711.
(12) Fuhrhop, J.-H.; Besecke, S.; Subramanian, J.; Mengersen, Chr.; Riesner, D. *J. Am. Chem. Soc.* **1975**, *97*, 7141.

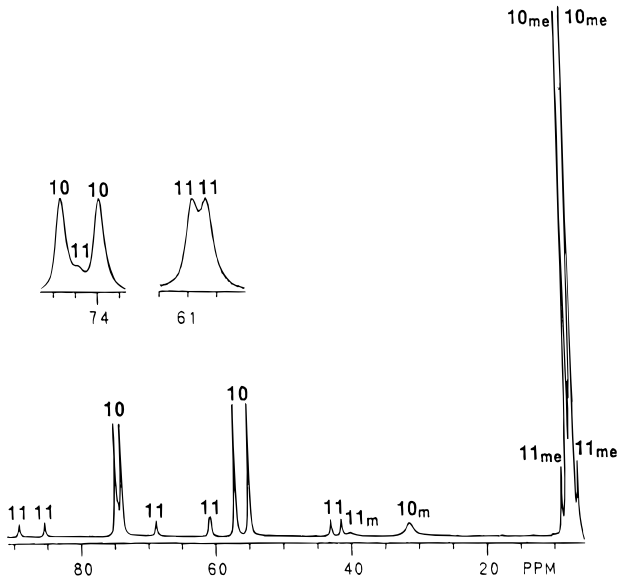

Figure 1. 300 MHz ^{1}H NMR spectrum of an isomeric mixture of BrFe^{III}(*trans*-OEPO$_2$) (**10a**) and BrFe^{III}(*cis*-OEPO$_2$) (**11a**) in chloroform-*d* at 25 °C. The porphyrin proton resonances are labeled with the subscripts m (meso), me (methyl), and no subscript (methylene). The insets show expansions of poorly resolved resonances in the methylene region of the spectrum.

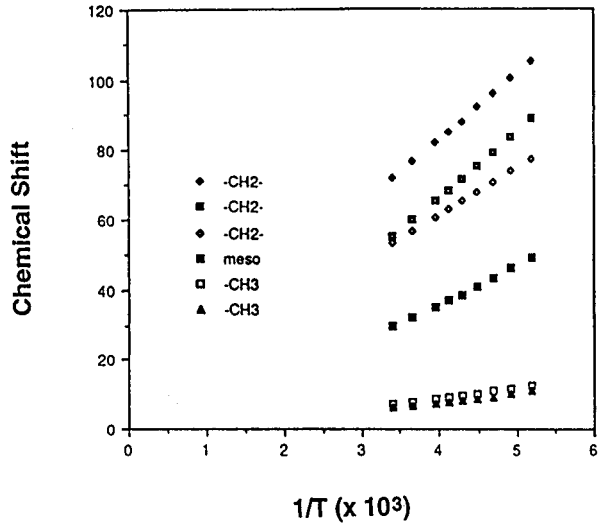

Figure 2. Curie plot of the chemical shifts of all resonances of ClFe^{III}(*trans*-OEPO$_2$) in dichloromethane-d_2 vs inverse temperature (K^{-1}). Two diastereotopic downfield methylene resonances are coincident in dichloromethane-d_2.

in Figure 1 show methylene resonances which are only partially resolved. Each isomer possesses only one type of meso proton. Characteristically, the resonances of the meso protons, which are closer to the paramagnetic iron center, are broader than the methylene resonances.[13] The methyl group resonances are crowded into a relatively narrow chemical shift range (6−9 ppm). As seen in Figure 1, the pair of methyl resonances designated **10** can easily be distinguished by their greater intensity. Only two of the anticipated four methyl resonances for **11a**, labeled **11**, can be discerned. The other two signals are probably hidden beneath the resonances from **10a**. The temperature dependence of the chemical shifts of **10b** is shown in the Curie plot in Figure 2. These plots show the slight curvature that is also observed for other high-spin iron(III) complexes.[14,15]

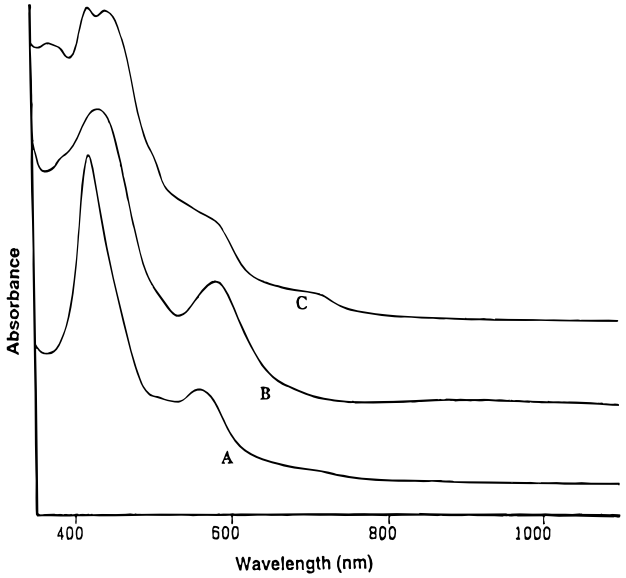

Figure 3. Electronic absorption spectra of pyridine solutions (>90% isomeric purity): (A) ClFe^{III}(*trans*-OEPO$_2$); (B) {Fe^{III}(*trans*-OEPO$_2$)}$_2$O; (C) (py)$_2$Fe^{II}(*trans*-OEPO$_2$).

The high spin ($S = {}^5/_2$) natures of **10** and **11** have been established by magnetic susceptibility and electron spin resonance spectral measurements. The magnetic moment of a mixture of **10b** and **11b** in chloroform solution at 25 °C is 5.8-(2) μ_B. The EPR spectra of these complexes do not show resolution of features for the two isomers. The spectrum obtained from the bromide complexes, **10a** and **11a**, in a frozen dichloromethane solution at 4.2 K shows a typical high-spin, five-coordinate iron(III) pattern with signals at $g = 6.2$ and 2.1. The $g = 2.1$ signal exhibits a partially resolved four-line pattern which results from hyperfine coupling to the axial bromide ligand with $A = 19(2)$ G. This Fe−Br coupling constant is smaller than the 28 G couplings found in (Br)Fe^{III}(OEPOH)[13] and (Br)Fe^{III}(protoporphyrin IX dimethyl ester).[16]

The electronic absorption spectrum of **10b** (> 90% isomeric purity obtained from {Fe^{III}(*trans*-OEPO$_2$)}$_2$O, **12**, *vide infra*) in pyridine solution shows a typical high-spin, five-coordinate iron(III) spectrum with a Soret band at 424 nm and less intense band at 562 nm (see Figure 3). The infrared spectrum of solid **10b** shows a single intense carbonyl stretch at 1603 cm^{-1}. Electron impact mass spectra of an isomeric mixture of **10** and **11** for both the bromo and chloro complexes reveal peaks with the largest mass and greatest intensity at $m/z = 618$ amu. This peak corresponds to Fe(*trans*-OEPO$_2$) and results in both cases from the loss of the axial halogen ligand. Other prominent peaks are observed at 603 and 589 amu; these correspond to the loss of a methyl and an ethyl group from Fe(*trans*-OEPO$_2$).

Crystal and Molecular Structure of ClFe^{III}(*trans*-OEPO$_2$)·1.5benzene, 10b. The structure of the complex has been determined by X-ray crystallography. Single crystals of **10b** that were suitable for X-ray diffraction were grown by slow diffusion of *n*-hexane into a benzene solution of **10b** and **11b**. The compound crystallizes with one molecule of the complex and 1.5 molecules of benzene in the asymmetric unit. Table 1 contains the atomic coordinates. Selected interatomic distances and angles are given in Table 2. The molecular structure is shown in Figure 4. The iron has five-coordinate geometry, and its structural features are consistent with those found for other high-spin, five-coordinate iron(III) porphyrin complexes.[17,18] The

(13) Balch, A. L.; Latos-Grażyński, L.; Noll, B. C.; Olmstead, M. M.; Zovinka, E. P. *Inorg. Chem.* **1992**, *31*, 2248.
(14) Walker, F. A.; La Mar, G. N. *Ann. N.Y. Acad. Sci.* **1973**, *206*, 328.
(15) La Mar, G. N.; Walker, F. A. *J. Am. Chem. Soc.* **1973**, *95*, 6950.
(16) Van Camp, H. L.; Scholes, C. P.; Mulks, C. F. *J. Am. Chem. Soc.* **1976**, *98*, 4094.

Table 1. Atomic Coordinates ($\times 10^4$) and Equivalent Isotropic Displacement Coefficients ($Å^2 \times 10^3$) for $ClFe^{III}$(*trans*-$OEPO_2$)·$1.5C_6H_6$

	x	*y*	*z*	*U*(eq)[a]
Fe	9742(1)	6919(1)	715(1)	13(1)
Cl	9763(2)	8088(1)	741(1)	19(1)
O(1)	13227(4)	6654(3)	1252(3)	34(2)
O(2)	6260(4)	6934(3)	175(3)	39(2)
N(1)	10812(4)	6694(3)	−57(4)	13(2)
N(2)	10806(4)	6676(3)	1817(4)	13(2)
N(3)	8655(5)	6707(3)	1475(4)	15(2)
N(4)	8651(4)	6744(3)	−396(4)	13(2)
C(1)	10653(6)	6665(4)	−993(5)	14(2)
C(2)	11562(6)	6557(4)	−1302(5)	16(2)
C(3)	12288(6)	6516(4)	−563(5)	18(2)
C(4)	11800(6)	6606(4)	189(5)	18(2)
C(5)	12313(6)	6631(4)	1114(5)	25(2)
C(6)	11811(6)	6637(4)	1881(5)	17(2)
C(7)	12282(6)	6568(4)	2783(5)	29(2)
C(8)	11558(6)	6585(4)	3286(5)	20(2)
C(9)	10651(6)	6648(4)	2688(5)	14(2)
C(10)	9731(5)	6647(4)	2937(5)	16(2)
C(11)	8806(6)	6655(4)	2413(5)	14(2)
C(12)	7894(6)	6632(4)	2727(5)	16(2)
C(13)	7165(6)	6673(4)	1993(5)	23(2)
C(14)	7645(6)	6719(4)	1237(5)	17(2)
C(15)	7156(6)	6797(4)	313(5)	20(2)
C(16)	7649(6)	6729(4)	−452(5)	18(2)
C(17)	7168(6)	6652(4)	−1353(5)	15(2)
C(18)	7897(5)	6634(4)	−1859(5)	14(2)
C(19)	8812(6)	6692(4)	−1265(5)	13(2)
C(20)	9725(6)	6680(4)	−1518(5)	16(2)
C(21)	11656(6)	6474(4)	−2258(5)	22(2)
C(22)	11463(6)	5731(4)	−2597(5)	33(2)
C(23)	13342(6)	6313(4)	−557(5)	22(2)
C(24)	13549(6)	5553(4)	−259(5)	29(2)
C(25)	13409(7)	6362(5)	3154(6)	53(3)
C(26)	13897(8)	7025(5)	3249(7)	72(3)
C(27)	11679(6)	6526(4)	4282(5)	21(2)
C(28)	11538(6)	5787(4)	4602(5)	40(2)
C(29)	7782(6)	6563(4)	3681(4)	17(2)
C(30)	7799(6)	5817(4)	4000(5)	41(2)
C(31)	6068(6)	6645(4)	1991(5)	26(2)
C(32)	5626(6)	5936(4)	1677(5)	38(2)
C(33)	6079(5)	6568(4)	−1684(5)	21(2)
C(34)	5715(6)	5838(4)	−1477(5)	31(2)
C(35)	7799(6)	6519(4)	−2851(5)	21(2)
C(36)	7955(6)	5763(4)	−3104(5)	33(2)
C(37)	5305(7)	8552(5)	489(6)	52(3)
C(38)	5364(7)	9263(5)	716(6)	49(3)
C(39)	4671(7)	9543(5)	1179(6)	51(3)
C(40)	3939(7)	9117(5)	1404(6)	51(3)
C(41)	3895(8)	8427(5)	1168(6)	51(3)
C(42)	4583(7)	8159(5)	722(6)	48(2)
C(43)	943(7)	4953(5)	472(6)	45(3)
C(44)	154(7)	5107(5)	903(6)	39(2)
C(45)	−772(7)	5141(5)	434(6)	44(3)

[a] Equivalent isotropic *U* defined as one-third of the trace of the orthogonalized $\mathbf{U}_{ij}$ tensor.

Table 2. Bond Lengths (Å) and Angles (deg) for $ClFe^{III}$(*trans*-$OEPO_2$)·$1.5C_6H_6$

Bond Lengths			
Fe−Cl	2.232(2)	Fe−N(1)	2.080(7)
Fe−N(2)	2.081(5)	Fe−N(3)	2.081(7)
Fe−N(4)	2.086(5)	O(1)−C(5)	1.240(10)
O(2)−C(15)	1.243(10)	N(1)−C(1)	1.405(9)
N(1)−C(4)	1.357(10)	N(2)−C(6)	1.372(10)
N(2)−C(9)	1.380(9)	N(3)−C(11)	1.410(9)
N(3)−C(14)	1.376(10)	N(4)−C(16)	1.368(10)
N(4)−C(19)	1.380(10)	C(1)−C(2)	1.425(11)
C(1)−C(3)	2.252(11)	C(1)−C(4)	2.183(9)
C(1)−C(20)	1.386(10)	C(2)−C(3)	1.373(9)
C(2)−C(4)	2.238(10)	C(3)−C(4)	1.434(11)
C(4)−C(5)	1.464(10)	C(5)−C(6)	1.455(12)
C(6)−C(7)	1.420(10)	C(6)−C(8)	2.227(11)
C(6)−C(9)	2.176(11)	C(7)−C(8)	1.358(12)
C(7)−C(9)	2.231(12)	C(8)−C(9)	1.418(10)
C(9)−C(10)	1.382(11)	C(10)−C(11)	1.382(10)
C(11)−C(12)	1.418(11)	C(11)−C(13)	2.239(11)
C(11)−C(14)	2.188(10)	C(12)−C(13)	1.369(10)
C(12)−C(14)	2.239(10)	C(13)−C(14)	1.423(12)
C(14)−C(15)	1.459(10)	C(15)−C(16)	1.449(12)
C(16)−C(17)	1.425(10)	C(16)−C(18)	2.233(11)
C(16)−C(19)	2.186(12)	C(17)−C(18)	1.366(11)
C(17)−C(19)	2.245(11)	C(18)−C(19)	1.422(10)
C(19)−C(20)	1.377(11)		

Bond Angles			
Cl−Fe−N(1)	102.0(2)	Cl−Fe−N(2)	101.7(2)
N(1)−Fe−N(2)	86.5(2)	Cl−Fe−N(3)	101.1(2)
N(1)−Fe−N(3)	156.9(2)	N(2)−Fe−N(3)	89.0(2)
Cl−Fe−N(4)	100.3(2)	N(1)−Fe−N(4)	89.5(2)
N(2)−Fe−N(4)	158.0(2)	N(3)−Fe−N(4)	86.2(2)
Fe−N(1)−C(1)	125.3(5)	Fe−N(1)−C(4)	130.0(5)
C(1)−N(1)−C(4)	104.4(6)	Fe−N(2)−C(6)	129.1(5)
Fe−N(2)−C(9)	125.4(5)	C(6)−N(2)−C(9)	104.5(5)
Fe−N(3)−C(11)	125.5(5)	Fe−N(3)−C(14)	129.9(5)
C(11)−N(3)−C(14)	103.5(6)	Fe−N(4)−C(16)	129.2(5)
Fe−N(4)−C(19)	125.2(5)	C(16)−N(4)−C(19)	105.4(6)
N(1)−C(1)−C(2)	110.3(6)	N(1)−C(1)−C(20)	123.5(7)
C(2)−C(1)−C(20)	126.0(7)	C(4)−C(1)−C(20)	160.2(7)
C(1)−C(2)−C(3)	107.2(6)	C(2)−C(3)−C(4)	105.7(7)
N(1)−C(4)−C(3)	112.3(6)	N(1)−C(4)−C(5)	123.8(7)
C(3)−C(4)−C(5)	123.8(7)	O(1)−C(5)−C(4)	118.2(8)
O(1)−C(5)−C(6)	118.2(7)	C(4)−C(5)−C(6)	123.6(7)
N(2)−C(6)−C(5)	123.8(6)	N(2)−C(6)−C(7)	111.2(7)
C(5)−C(6)−C(7)	125.0(7)	C(5)−C(6)−C(9)	161.6(6)
C(6)−C(7)−C(8)	106.6(7)	C(7)−C(8)−C(9)	106.9(7)
N(2)−C(9)−C(8)	110.8(7)	N(2)−C(9)−C(10)	124.2(6)
C(8)−C(9)−C(10)	124.9(7)	C(9)−C(10)−C(11)	129.7(7)
N(3)−C(11)−C(10)	123.1(7)	N(3)−C(11)−C(12)	111.0(6)
C(10)−C(11)−C(12)	125.9(7)	C(11)−C(12)−C(13)	106.9(7)
C(12)−C(13)−C(14)	106.6(7)	N(3)−C(14)−C(13)	112.0(6)
N(3)−C(14)−C(15)	122.2(7)	C(13)−C(14)−C(15)	125.7(7)
O(2)−C(15)−C(14)	117.7(7)	O(2)−C(15)−C(16)	118.0(6)
C(14)−C(15)−C(16)	124.2(7)	N(4)−C(16)−C(15)	123.7(6)
N(4)−C(16)−C(17)	111.0(7)	C(15)−C(16)−C(17)	125.3(7)
C(16)−C(17)−C(18)	106.3(6)	C(17)−C(18)−C(19)	107.2(6)
N(4)−C(19)−C(18)	110.1(7)	N(4)−C(19)−C(20)	124.9(6)
C(18)−C(19)−C(20)	124.9(7)	C(1)−C(20)−C(19)	129.4(7)

Fe−N distances are between 2.080(7) and 2.086(5) Å and are within the 2.060(3)−2.087(8) Å range expected for this class of molecule. The iron atom sits 0.41 Å above the mean N_4 plane which is also in the expected range of 0.39−0.54 Å seen previously. Likewise, the Fe−Cl distance of 2.232(2) Å is similar to the distances found in $ClFe^{III}$(OEPOAc) (2.236(2) Å)[13] and $ClFe^{III}$(protoporphyrin IX dimethyl ester) (2.218(6) Å).[19]

The dioxoporphodimethene ligand shows some interesting structural differences from typical porphyrin ligands. The carbon−oxygen bond lengths of 1.243(10) and 1.240(10) Å are clearly indicative of double bond character. These compare well with the carbon−oxygen bond lengths of 1.220(9) and 1.235(9) Å found in $ClTl^{III}$(*trans*-$OEPO_2$).[20] The sum of the angles at the two oxidized bridgehead carbons is 360.0(7)° for C(5) and 359.9(7)° for C(15). The porphyrin skeleton bond angles of the oxidized meso carbons C(4)−C(5)−C(6) and C(14)−C(15)−C(16) are 123.6(7) and 124.(7)°, respectively. The remaining pair of meso carbons show larger skeletal bond angles of 129.9(7)° for C(9)−C(10)−C(11) and 129.4(7)° for C(1)−C(20)−C(19). These angles can be compared to the mean values found in $ClFe^{III}$(protoporphyrin IX dimethyl ester)[19] (125.9°) and $ClFe^{III}$(OEPOAc)[13] (127.5(5)°). The dioxopor-

(17) Scheidt, W. R., Reed, C. A. *Chem. Rev.* **1981**, *81*, 543.
(18) Scheidt, W. R., Lee, Y. J. *Struct. Bonding* **1987**, *64*, 1.
(19) Koenig, D. F. *Acta Crystallogr.* **1965**, *18*, 663.
(20) Senge, M. O.; Smith, K. M. *Z. Naturforsch.* **1992**, *47B*, 837.

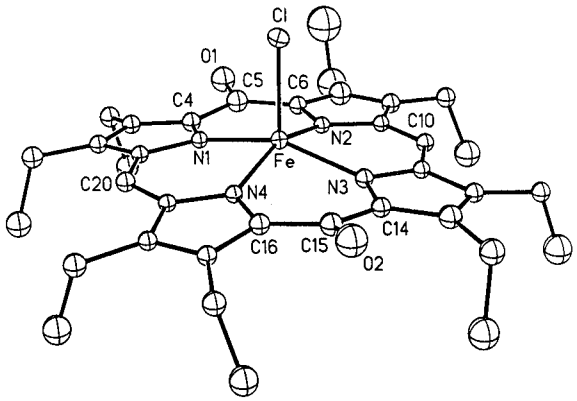

Figure 4. Perspective view of $ClFe^{III}$(*trans*-$OEPO_2$) with 50% thermal contours. The numbering of the 20 carbon atoms of the porphyrin core is sequential, 1−20, but for clarity only selected carbon atoms are numbered.

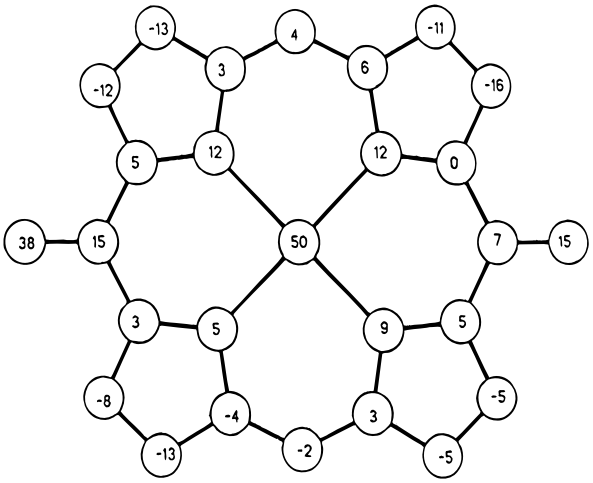

Figure 5. Diagram of the macrocyclic core of $ClFe^{III}$(*trans*-$OEPO_2$). Each atom symbol has been replaced by a number representing the perpendicular displacement in 0.01 Å units from the mean plane of the core.

phodimethene macrocycle appears to elongate toward the oxidized meso carbons. The C(5)···C(15) distance between the oxidized meso carbons is 7.001 Å, whereas the comparable C(10)···C(20) distance is 6.777 Å. The $C_{meso}-C_{\alpha}$ bond lengths of the oxidized meso carbons have a longer mean value of 1.457(11) Å compared to the other pair of meso carbon atoms which have mean $C_{meso}-C_{\alpha}$ values of 1.382(11) Å. Both $ClFe^{III}$(protoporphyrin IX dimethyl ester)[19] and $ClFe^{III}$(OEPOAc)[13] have mean $C_{meso}-C_{\alpha}$ bond lengths of 1.38 Å. This agrees with the trend seen for $ClTl^{III}$(*trans*-$OEPO_2$),[20] which has mean $C_{meso}-C_{\alpha}$ distances of 1.483(8) and 1.400(9) Å for the respective types of meso carbons.

The dioxoporphodimethene macrocycle is slightly domed as quantitatively illustrated in Figure 5 which shows the displacements (in 0.01 Å) of each atom from the mean dioxoporphodimethene plane. The oxygen atoms bend 0.38 Å (O1) and 0.15 Å (O2) back away from the mean macrocyclic plane. This differs from the structure of ClTl(*trans*-$OEPO_2$),[20] which, despite having five-coordinate geometry, shows a slight ruffling of the macrocycle. Additionally in the thallium complex, the oxygen atoms are displaced on opposite sides of the mean dioxoporphodimethene plane.

The molecular packing within the solid shows some interesting interactions between the macrocyclic complexes and the benzene molecules. As shown in Figure 6, benzene molecules nestle between the faces of two monomeric complexes so that the appended ethyl groups create a cage about these benzene

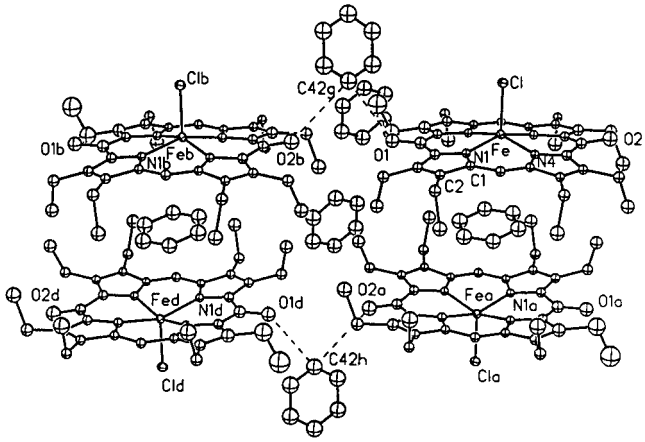

Figure 6. View of the orientations of molecules of benzene and $ClFe^{III}$(*trans*-$OEPO_2$) in the solid, $ClFe^{III}$(*trans*-$OEPO_2$)·1.5benzene.

molecules. Other benzene molecules are arranged so that para C-H groups interact with the oxygen atoms of two different dioxo-porphodimethene ligands. The relevant O···H distances are 2.96 (O(1)−H(42)) and 2.89 Å (O(2)−H(42) with an O···H···O angle of 109.1°). These interactions between the two molecular components are likely to be important in creating an ordered structure for this solid. In contrast, many peripherally modified derivatives of octaethylporphyrin show orientational disorder because the modifications are hidden by the protruding ethyl groups on the molecular surface.[3,5,6]

Formation and Spectroscopic Characterization of the (μ-Oxo)iron(III) Dimer. {Fe^{III}(*trans*-$OEPO_2$)}$_2$O, **12**, is synthesized by washing a dichloromethane solution of the monomers **10** and **11** with aqueous sodium hydroxide followed by isolation from the organic layer. Chromatography of **10** and **11** on neutral alumina with dichloromethane eluant also converts a significant portion (∼85%) of the monomer to the μ-oxo form. Successive fractional crystallizations of the mixture of μ-oxo isomers from dichloromethane by slow diffusion of ethanol yields {Fe^{III}(*trans*-$OEPO_2$)}$_2$O in greater than 90% isomeric purity. The electronic absorption spectrum of **12** (Figure 3) in pyridine shows two

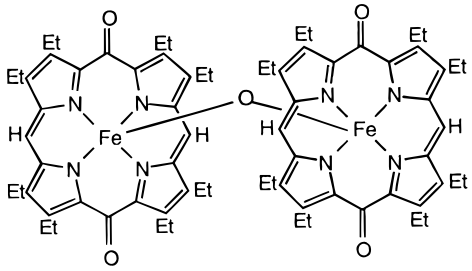

12, {Fe^{III}(*trans*-$OEPO_2$)}$_2$O

broad bands at 436 and 584 nm. An intense C−O stretch at 1590 cm^{-1} is present in the infrared spectrum of the solid. Like the monomeric complexes, **12** gives an electron impact mass spectra which contains a highest mass, greatest intensity peak at m/z = 618 amu that corresponds to an iron dioxoporphodimethene unit.

Figure 7 shows the ^{1}H NMR spectrum of an isomeric mixture of the (μ-oxo)iron(III) complexes in chloroform solution. Each iron dioxoporphodimethene unit within the dimer should possess the same microsymmetry as the corresponding five-coordinate monomer. Thus, **12** gives rise to four methylene proton resonances at 4.24, 4.81, 5.40, and 6.29 ppm, one meso resonance at 6.60 ppm, and two methyl resonances at 1.00 and 1.16 ppm. The other low intensity peaks seen in the methylene and meso region of the spectrum from 3.5 to 7.0 ppm likely

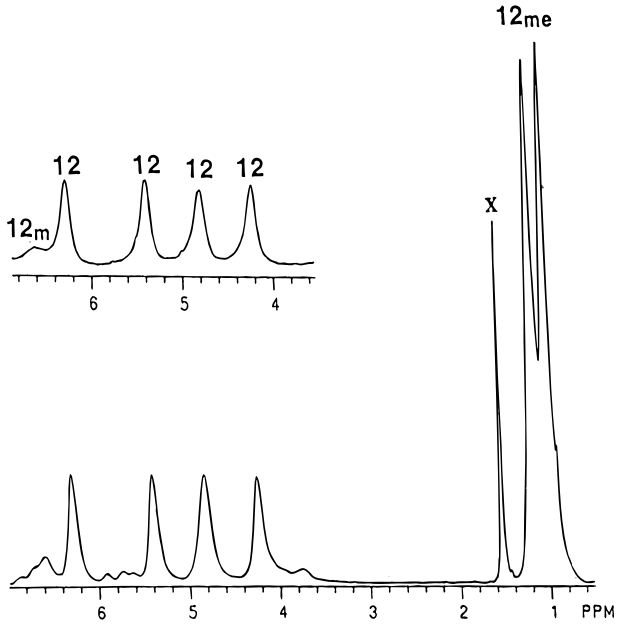

Figure 7. ^{1}H NMR spectrum of a mixture of isomers of {Fe^{III}(OEPO$_2$)}$_2$O in chloroform-*d* at 25 °C. The porphyrin proton resonances are labeled with the subscripts m (meso), me (methyl), and no subscript (methylene); X is due to water. The inset shows a sample which has >90% isomeric purity of the *trans* compound, **12**.

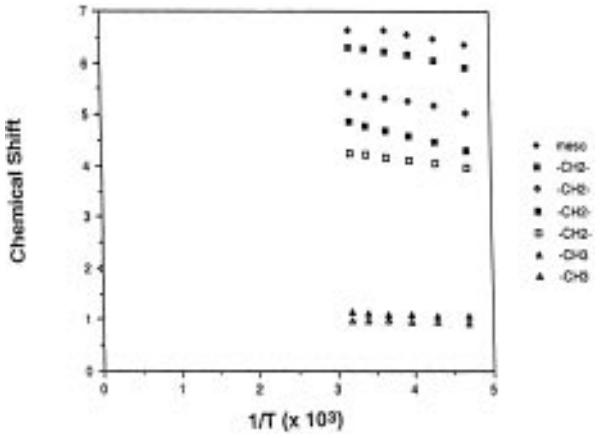

Figure 8. Curie plot showing temperature dependence (K^{-1}) of chemical shifts for {Fe^{III}(*trans*-OEPO$_2$)}$_2$O in chloroform-*d*.

arise from dimers containing other possible isomeric mixtures of dimers. The amount of these dimers, relative to **12**, depended on the percentage of *cis* free base starting material initially present. The inset in Figure 7 shows a comparison of the methylene and meso resonances of a purified sample of **12.**

{Fe^{III}(*trans*-OEPO$_2$)}$_2$O contains two antiferromagnetically-coupled, high-spin iron(III) centers similar to the well-known (μ-oxo)iron(III) porphyrin dimers.[21] The broad ^{1}H NMR resonances all have chemical shifts which fall within the diamagnetic pocket. The Curie plot shown in Figure 8 clearly illustrates the antiferromagnetic nature of the chemical shifts with temperature. The magnetic susceptibility of **12** in chloroform solution at 298 K is 1.9(2) μ_B, which is similar to the room temperature moment of 1.8−1.9 μ_B found for {Fe(TPP)}$_2$O.[21]

Acidification of a solution of purified {Fe^{III}(*trans*-OEPO$_2$)}$_2$O with hydrogen chloride yields ClFe^{III}(*trans*-OEPO$_2$) in greater than 90% purity. A sample of ClFe^{III}(*trans*-OEPO$_2$) prepared in this fashion was used to record the UV/vis spectrum shown in Figure 3.

(21) La Mar, G. N.; Eaton, G. R.; Holm, R. H.; Walker, F. A. *J. Am. Chem. Soc.* **1973**, *95*, 63.

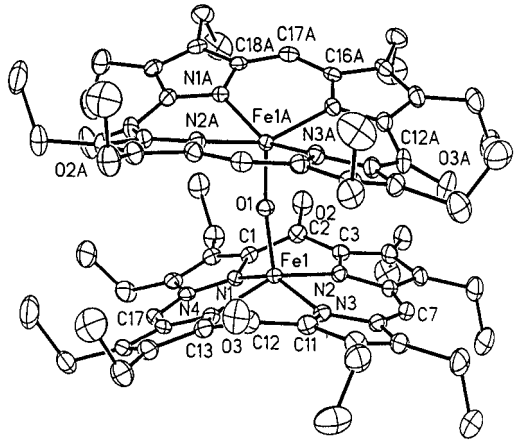

Figure 9. Perspective view of {Fe^{III}(*trans*-OEPO$_2$)}$_2$O showing 20% thermal contours. The numbering of the 20 carbon atoms of the porphyrin core is sequential, 1−20, but for clarity only selected carbon atoms are numbered.

Crystal and Molecular Structure of {Fe^{III}(*trans*-OEPO$_2$)}$_2$O, 12. Single crystals suitable for diffraction were grown by slow diffusion of isooctane into a dichloromethane solution of **12**. {Fe^{III}(*trans*-OEPO$_2$)}$_2$O crystallizes with a crystallographically imposed 2-fold axis of symmetry that passes through the oxo ligand. A view of **12** is shown in Figure 9. Table 3 contains the atomic coordinates. Selected interatomic distances and angles are given in Table 4 .

The five-coordinate geometry around the iron atom is similar to that for other high spin iron(III) derivatives.[17,18] The Fe−O distance of 1.749(1) Å falls in the typical range of 1.73−1.79 Å seen for other (μ-oxo)iron(III) porphyrins.[22,23] Likewise, **12** has a mean Fe−N distance of 2.077(3) Å which is also within the typical range of mean bond lengths (2.07−2.09 Å) seen previously.[22,23] However, the Fe−O−Fe angle of 165.4(2)° deviates significantly from linearity. The most acute Fe−O−Fe angle reported for porphyrin systems is 161.1(4)° in Fe$_2$(FF)(μ-O)·H$_2$O (where FF is bis(5-(*o*-phenyl)-10,15,20-triphenylporphyrin)urea)[23] which contains an additional covalent urea link between the periphery of each porphyrin in the dimer. Other reported (μ-oxo)iron(III) porphyrins have Fe−O−Fe angles ranging from 173−179°.[17,18]

The carbon−oxygen bond lengths in **12** are 1.221(6) and 1.223(6) Å. These distances indicate the double bond character of these groups and are in agreement with similar bond lengths found in ClFe^{III}(*trans*-OEPO$_2$) (1.242(10) Å) and ClTl^{III}(*trans*-OEPO$_2$)[20] (1.228(9) Å). The sum of angles around the keto bridgehead carbon atom is 359.8° for C(2) and 360.0° for C(12). The carbon skeleton at the oxygenated meso carbon atoms appears to pinch together as indicated by narrower C(1)−C(2)−C(3) and C(11)−C(12)−C(13) angles of 119.9(4) and 120.1(4)°, respectively. The other pair of meso carbons show broader skeletal angles of 128.9(4) and 129.3(4)°. This trend is also seen for ClFe^{III}(*trans*-OEPO$_2$) and ClTl^{III}(*trans*-OEPO$_2$).[20] Longer C$_{meso}$−C $_\alpha$ bond lengths for the keto meso carbons are observed in **12** with a mean distance of 1.472(6) Å which compare well with the distances found in ClFe^{III}(*trans*-OEPO$_2$) (1.457(11) Å) and ClTl^{III}(*trans*-OEPO$_2$)[20] (1.483(8) Å). The other pair of meso carbons have mean C$_{meso}$−C$_\alpha$ distances of 1.377(6) Å, typical of other porphyrin systems. Consequently the C2···C12 distance between the oxidized meso carbons (6.818 Å) is longer than the C7···C17 distance between the remaining pair of meso carbons (6.602 Å).

(22) Lay, K.-L.; Buchler, J. W.; Kenny, J. E.; Scheidt, W. R. *Inorg. Chim. Acta* **1986**, *123*, 91.
(23) Landrum, J. T.; Grimmett, D.; Haller, K. J.; Scheidt, W. R.; Reed, C. A. *J. Am. Chem. Soc.* **1981**, *103*, 2640.

Table 3. Atomic Coordinates ($\times 10^4$) and Equivalent Isotropic Displacement Coefficients ($Å^2 \times 10^3$) for $[Fe^{III}(trans\text{-}OEPO_2)]_2O$

	x	*y*	*z*	*U*(eq)[a]
Fe(1)	293(1)	693(1)	3352(1)	36(1)
O(1)	0	549(2)	2500	45(1)
O(2)	1543(2)	−1404(2)	2629(2)	90(2)
O(3)	−1119(2)	2714(2)	3520(3)	95(2)
N(1)	427(1)	−560(2)	3712(2)	41(1)
N(2)	1167(1)	722(2)	3185(2)	43(1)
N(3)	325(1)	2035(2)	3485(2)	44(1)
N(4)	−423(1)	749(2)	3998(2)	44(1)
C(1)	825(2)	−1126(3)	3460(2)	46(2)
C(2)	1298(2)	−862(3)	2994(3)	55(2)
C(3)	1501(2)	41(3)	3007(2)	46(1)
C(4)	2070(2)	310(3)	2863(3)	56(2)
C(5)	2077(2)	1192(3)	2957(3)	54(2)
C(6)	1516(2)	1449(3)	3144(2)	46(1)
C(7)	1330(2)	2282(3)	3251(2)	50(2)
C(8)	788(2)	2577(3)	3399(2)	47(2)
C(9)	610(2)	3464(3)	3425(3)	57(2)
C(10)	32(2)	3462(3)	3494(3)	62(2)
C(11)	−130(2)	2569(3)	3539(3)	51(2)
C(12)	−711(2)	2257(3)	3668(3)	59(2)
C(13)	−804(2)	1406(3)	4017(3)	50(2)
C(14)	−1299(2)	1168(3)	4426(3)	60(2)
C(15)	−1213(2)	333(3)	4646(3)	54(2)
C(16)	−666(2)	69(3)	4370(2)	45(1)
C(17)	−425(2)	−740(3)	4438(2)	51(2)
C(18)	67(2)	−1055(3)	4131(2)	44(1)
C(19)	259(2)	−1936(3)	4155(3)	52(2)
C(20)	734(2)	−1983(3)	3724(3)	52(2)
C(21)	2568(2)	−277(4)	2691(3)	79(2)
C(22)	2782(3)	−764(4)	3338(4)	113(3)
C(23)	2580(2)	1789(3)	2900(3)	78(2)
C(24)	2866(3)	1960(5)	2584(4)	120(3)
C(25)	1002(3)	4229(3)	3388(3)	79(2)
C(26)	1265(3)	4459(4)	4098(4)	123(4)
C(27)	−372(3)	4252(3)	3486(4)	92(3)
C(28)	−573(3)	4433(4)	4205(4)	117(3)
C(29)	−1797(2)	1747(4)	4603(3)	81(2)
C(30)	−2263(3)	1687(5)	4069(4)	121(4)
C(31)	−1607(2)	−241(4)	5058(3)	76(2)
C(32)	−1977(3)	−778(5)	4582(4)	127(4)
C(33)	−27(3)	−2650(3)	4559(3)	77(2)
C(34)	−525(3)	−3030(4)	4165(4)	118(3)
C(35)	1083(2)	−2780(3)	3579(3)	80(2)
C(36)	883(3)	−3249(4)	2925(4)	103(3)

[a] Equivalent isotropic *U* defined as one-third of the trace of the orthogonalized $\mathbf{U}_{ij}$ tensor.

Figure 10 shows the displacements (in 0.01 Å) of each atom from the mean dioxoporphodimethene plane. The pronounced ruffling of the macrocyclic core is clearly evident. The iron is sitting 0.60 Å out of the mean plane of the macrocycle, which is slightly longer than typical high-spin, five-coordinate iron(III) porphyrins.[17,18] This characteristic is also found in $Fe_2(FF)(\mu\text{-}O)\cdot H_2O$[23] which has iron displacements of 0.60 and 0.65 Å for the two distinct halves of the dimer.

The macrocyclic ligands are roof-shaped and fold away from each other. The oxygen functionalities on the ligands bend back towards the cavity of the dimer and are related by an idealized S_4 symmetry operation. The two macrocyclic ligands are not coplanar but form a dihedral angle of 13.5°. The closest interatomic distance between the two ligands is 3.89 Å, (C(7)−C(12A)), and the perpendicular separation between the two mean cores ranges from 3.47 to 5.87 Å.

Autoreduction of Iron(III) Complexes in Pyridine To Form $(py)_2Fe^{II}(trans\text{-}OEPO_2)$, 13. Dissolution of **10a,b** or **12** (>90% isomeric purity) in pyridine over the course of 1 week at room temperature afforded $(py)_2Fe^{II}(trans\text{-}OEPO_2)$, **13**. Heating the solution speeds up the time course for the reaction so that at 65 °C complete conversion is realized in 1 day. Immediate conversion is accomplished by addition of ascorbic acid to the pyridine solutions. Figure 3 shows the electronic absorption spectrum for pyridine solutions of **13** in trace C. The spectrum of **13** shows a split Soret band with peaks at 425 and 447 nm. Several shoulders are also apparent on the low energy side of the Soret at 504, 582, and 712 nm. Solid samples of **13** show a strong C−O stretch in the infrared spectrum at 1592 cm^{-1}.

Table 4. Bond Lengths (Å) and Angles (deg) for $\{(OEPO_2)Fe^{III}\}_2O$

Bond Lengths			
Fe(1)−O(1)	1.749(1)	Fe(1)−N(1)	2.067(3)
Fe(1)−N(2)	2.083(3)	Fe(1)−N(3)	2.081(3)
Fe(1)−N(4)	2.075(3)	O(1)−Fe(1A)	1.749(1)
O(2)−C(2)	1.223(6)	O(3)−C(12)	1.221(6)
N(1)−C(1)	1.364(5)	N(1)−C(18)	1.383(5)
N(2)−C(3)	1.351(5)	N(2)−C(6)	1.391(5)
N(3)−C(8)	1.383(5)	N(3)−C(11)	1.355(6)
N(4)−C(13)	1.354(5)	N(4)−C(16)	1.381(5)
C(1)−C(2)	1.471(6)	C(1)−C(20)	1.424(6)
C(2)−C(3)	1.469(6)	C(3)−C(4)	1.429(6)
C(4)−C(5)	1.368(7)	C(5)−C(6)	1.421(6)
C(6)−C(7)	1.371(6)	C(7)−C(8)	1.381(6)
C(8)−C(9)	1.428(6)	C(9)−C(10)	1.367(7)
C(10)−C(11)	1.430(6)	C(11)−C(12)	1.469(6)
C(12)−C(13)	1.480(6)	C(13)−C(14)	1.441(6)
C(14)−C(15)	1.364(7)	C(15)−C(16)	1.445(6)
C(16)−C(17)	1.374(6)	C(17)−C(18)	1.381(6)
C(18)−C(19)	1.429(6)	C(19)−C(20)	1.380(7)
Bond Angles			
O(1)−Fe(1)−N(1)	103.7(2)	O(1)−Fe(1)−N(2)	104.7(1)
N(1)−Fe(1)−N(2)	85.3(1)	O(1)−Fe(1)−N(3)	104.4(2)
N(1)−Fe(1)−N(3)	151.9(1)	N(2)−Fe(1)−N(3)	87.8(1)
O(1)−Fe(1)−N(4)	102.4(1)	N(1)−Fe(1)−N(4)	88.4(1)
N(2)−Fe(1)−N(4)	152.8(1)	N(3)−Fe(1)−N(4)	85.4(1)
Fe(1)−O(1)−Fe(1A)	165.4(2)	Fe(1)−N(1)−C(1)	126.1(3)
Fe(1)−N(1)−C(18)	127.3(3)	C(1)−N(1)−C(18)	105.3(3)
Fe(1)−N(2)−C(3)	126.5(3)	Fe(1)−N(2)−C(6)	127.5(3)
C(3)−N(2)−C(6)	105.5(3)	Fe(1)−N(3)−C(8)	127.9(3)
Fe(1)−N(3)−C(11)	125.6(3)	C(8)−N(3)−C(11)	105.4(3)
Fe(1)−N(4)−C(13)	125.8(3)	Fe(1)−N(4)−C(16)	126.9(3)
C(13)−N(4)−C(16)	106.0(3)	N(1)−C(1)−C(2)	123.2(4)
N(1)−C(1)−C(20)	111.6(4)	C(2)−C(1)−C(20)	125.1(4)
O(2)−C(2)−C(1)	119.9(4)	O(2)−C(2)−C(3)	120.0(4)
C(1)−C(2)−C(3)	119.9(4)	N(2)−C(3)−C(2)	123.2(4)
N(2)−C(3)−C(4)	111.5(4)	C(2)−C(3)−C(4)	125.2(4)
C(3)−C(4)−C(5)	105.9(4)	C(4)−C(5)−C(6)	107.3(4)
N(2)−C(6)−C(5)	109.8(4)	N(2)−C(6)−C(7)	123.7(4)
C(5)−C(6)−C(7)	126.5(4)	C(6)−C(7)−C(8)	129.3(4)
N(3)−C(8)−C(7)	123.5(4)	N(3)−C(8)−C(9)	110.0(4)
C(7)−C(8)−C(9)	126.3(4)	C(8)−C(9)−C(10)	107.1(4)
C(9)−C(10)−C(11)	105.9(4)	N(3)−C(11)−C(10)	111.5(4)
N(3)−C(11)−C(12)	123.4(4)	C(10)−C(11)−C(12)	125.0(4)
O(3)−C(12)−C(11)	120.4(4)	O(3)−C(12)−C(13)	119.5(4)
C(11)−C(12)−C(13)	120.1(4)	N(4)−C(13)−C(12)	123.4(4)
N(4)−C(13)−C(14)	111.2(4)	C(12)−C(13)−C(14)	125.4(4)
C(13)−C(14)−C(15)	106.2(4)	C(14)−C(15)−C(16)	106.8(4)
N(4)−C(16)−C(15)	109.7(4)	N(4)−C(16)−C(17)	124.0(4)
C(15)−C(16)−C(17)	126.2(4)	C(16)−C(17)−C(18)	128.9(4)
N(1)−C(18)−C(17)	123.7(4)	N(1)−C(18)−C(19)	110.3(4)
C(17)−C(18)−C(19)	125.9(4)	C(18)−C(19)−C(20)	106.7(4)
C(1)−C(20)−C(19)	106.0(4)		

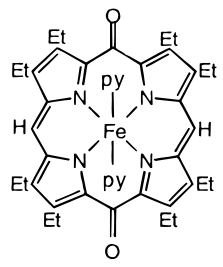

13, $(py)_2Fe^{II}(trans\text{-}OEPO_2)$

The ^1H NMR spectrum of **13** in pyridine-d_5 solution at 25 °C clearly indicates the diamagnetic nature of this compound.

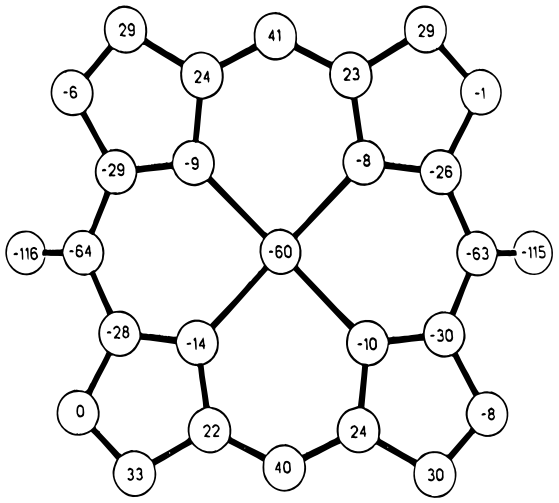

Figure 10. Diagram of the macrocylic core within $\{Fe^{III}(trans\text{-}OEPO_2)\}_2O$. Each atom symbol has been replaced by a number representing the perpendicular displacement, in units of 0.01 Å, from the mean plane of the core.

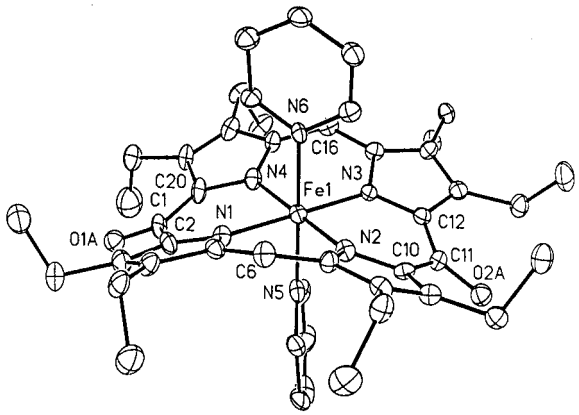

Figure 11. Perspective view of one molecule of $(py)_2Fe^{II}(trans\text{-}OEPO_2)$ with 20% thermal contours. The structure is depicted without showing the disorder inherent in the *trans* keto sites. The other independent molecule has a similar structure. The numbering of the 20 carbon atoms of the porphyrin core is sequential, 1−20, but for clarity only selected carbon atoms are numbered.

The axial coordination of the two pyridine ligands renders the macrocyclic faces magnetically equivalent. Consequently, the ethyl groups in **13** give rise to only two methylene quartet resonances centered at 2.58 and 3.08 ppm and a pair of methyl triplets centered at 1.14 and 1.36 ppm. The two equivalent meso protons give rise to a single resonance at 6.91 ppm.

Crystal and Molecular Structure of $(py)_2Fe^{II}(trans\text{-}OEPO_2)$, 13. Slow evaporation of a pyridine/water solution of **13** yielded crystals suitable for X-ray diffraction. The complex crystallized with two distinct molecules of **13** in the asymmetric unit. The meso oxygen atoms are disordered in *trans* positions on the ligands with 71/29 and 50/50% site occupancy for each of the two independent molecules. Disorder of the oxygen atoms for this type of complex is common.[8,24,25] Table 5 contains the atomic coordinates. Selected interatomic distances and angles are given in Table 6. Figure 11 shows a perspective drawing of **13**.

The six-coordinate iron atom bonds to four pyrrole nitrogen atoms and two axial pyridine ligands. The mean in-plane Fe−N(pyrrole) distance for each molecule (1.94, 1.96 Å) is on the short end of the corresponding mean range of distances (1.981(28)−2.108(12) Å) found in similar Fe(II) complexes.[17,18] The mean axial Fe−N(pyridine) distances of 1.97 and 1.99 Å in **13** are also slightly shorter than those found in $(py)_2Fe^{II}(TPP)$ (2.039(1) Å).[26] The mean range of bond lengths observed in comparable systems is 2.039(1)−2.127(3) Å.[19] The φ angles, (angle between the plane of the axial ligand and the closest Fe−N(pyrrole) bond), are both 35.1°. The two axial pyridine ligands on each complex lie in planes which are 74.6 and 75.3° apart. The cores of the two independent molecules show similar deviations of a severely ruffled macrocycle as is evident from the out-of-plane atomic displacements shown in Figure 12. However, the iron atom lies in the plane of the four macrocyclic nitrogen atoms. Both keto oxygen atoms protrude severely out to one side of the macrocyclic plane for each distinct molecule by an average of 0.14 Å. With due regard for disorder, the major C(1)−O(1), C(11)−O(2), C(52)−O(3) and C(62)−O(4) groups have mean bond distances of 1.27 Å. The minor sites have a mean bond length of 1.23 Å. These C−O distances are slightly longer those found for **10b**, **12**, and $ClTl^{III}(trans\text{-}OEPO_2)$[20] (1.221(6)−1.243(10) Å), but they are indicative of double bond character at these sites.

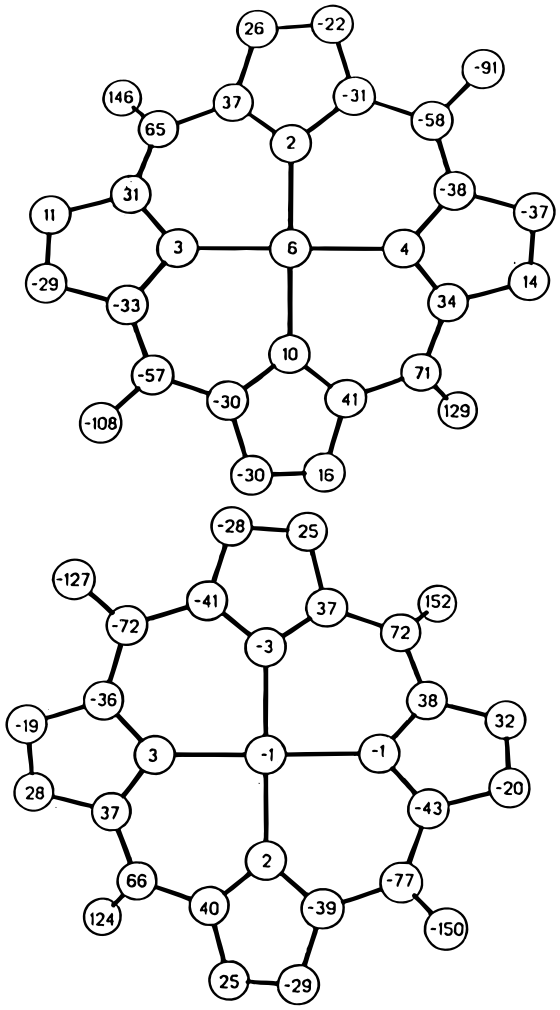

Figure 12. Diagrams of the macrocylic core of the two crystallographically distinct $(py)_2Fe^{II}(trans\text{-}OEPO_2)$ molecules in the unit cell. The disordered *trans* oxygen atom positions are included. Each atom symbol has been replaced by a number representing the perpendicular displacement, in units of 0.01 Å, from the mean plane of the core.

(24) Balch, A. L.; Noll, B. C.; Zovinka, E. P. *J. Am. Chem. Soc*, **1992**, *114*, 3380.
(25) Balch, A. L.; Chan, Y. W.; Olmstead, M. M.; Renner, M. W. *J. Am. Chem. Soc.* **1985**, *107*, 2393.
(26) Li, N.; Petricek, V.; Coppens, P.; Landrum, J. *Acta Crystallogr., Sect C*, **1985**, *C41*, 902.

Table 5. Atomic Coordinates ($\times 10^4$) and Equivalent Isotropic Displacement Parameters ($Å^2 \times 10^3$) for $(py)_2Fe^{II}$(*trans*-$OEPO_2$)

	x	*y*	*z*	*U*(eq)[a]		*x*	*y*	*z*	*U*(eq)[a]
Fe(1)	1240(1)	5700(1)	4945(1)	40(1)	Fe(2)	6189(1)	5551(1)	4896(1)	35(1)
O(1A)	617(5)	5768(5)	501(9)	57(2)	O(3A)	4466(7)	6117(7)	1567(13)	57(3)
O(2A)	2998(5)	5305(5)	8289(9)	57(2)	O(4A)	6837(7)	5388(8)	9317(14)	57(3)
O(1B)	−37(13)	3889(13)	5588(23)	57(2)	O(3B)	5765(7)	3304(8)	4379(14)	57(3)
O(2B)	1307(13)	7950(13)	5357(24)	57(2)	O(4B)	7441(7)	7446(8)	4570(13)	57(3)
N(1)	675(4)	5096(4)	3679(7)	44(2)	N(7)	6091(4)	6296(4)	3672(7)	38(2)
N(2)	1406(4)	4973(4)	6193(7)	44(2)	N(8)	5576(4)	5012(4)	3597(7)	38(2)
N(3)	1782(4)	6289(4)	6193(7)	37(2)	N(9)	6309(4)	4795(4)	6098(7)	37(2)
N(4)	1052(4)	6426(4)	3690(7)	47(2)	N(10)	6794(4)	6086(4)	6191(7)	37(2)
N(5)	2090(4)	5461(5)	4250(7)	50(2)	N(11)	7023(4)	5243(4)	4173(7)	37(2)
N(6)	381(4)	5925(4)	5651(6)	38(2)	N(12)	5339(4)	5843(4)	5576(7)	37(2)
C(1)	677(6)	5765(6)	1704(8)	52(3)	C(47)	7050(5)	6975(5)	4723(10)	46(3)
C(2)	520(5)	5166(5)	2387(10)	50(3)	C(48)	6529(5)	6844(5)	3701(8)	39(2)
C(3)	106(6)	4615(6	1826(10)	58(3)	C(49)	6304(5)	7279(6)	2601(10)	50(3)
C(4)	−14(5)	4214(5)	2856(10)	51(3)	C(50)	5732(6)	6995(5)	1929(10)	50(3)
C(5)	369(5)	4529(5)	4010(9)	44(2)	C(51)	5601(5)	6384(5)	2593(9)	38(2)
C(6)	456(5)	4229(5)	5246(10)	52(3)	C(52)	5059(5)	5917(5)	2173(9)	49(3)
C(7)	1013(5)	4415(5)	6250(9)	42(2)	C(53)	5112(4)	5229(5)	2564(9)	39(2)
C(8)	1257(5)	4011(5)	7360(10)	48(3)	C(54)	4736(4)	4677(5)	1873(9)	36(2)
C(9)	1846(5)	4316(5)	7987(10)	45(2)	C(55)	5006(5)	4112(5)	2498(9)	41(2)
C(10)	1934(5)	4921(4)	7226(9)	38(2)	C(56)	5507(5)	4323(5)	3578(9)	41(2)
C(11)	2412(5)	5442(5)	7623(9)	46(3)	C(57)	5842(6)	3914(5)	4600(9)	48(3)
C(12)	2279(5)	6126(5)	7221(9)	43(3)	C(58)	6191(5)	4130(5)	5766(9)	43(2)
C(13)	2587(5)	6710(5)	7863(10)	47(3)	C(59)	6383(5)	3701(5)	6894(10)	51(3)
C(14)	2256(5)	7237(5)	7251(10)	45(3)	C(60)	6578(5)	4117(5)	7931(9)	46(3)
C(15)	1772(5)	6985(5)	6207(10)	44(2)	C(61)	6539(5)	4798(5)	7388(9)	38(2)
C(16)	1436(5)	7368(5)	5148(10)	46(3)	C(62)	6781(5)	5384(5)	8141(9)	43(2)
C(17)	1130(5)	7099(5)	3946(9)	46(3)	C(63)	6990(5)	5981(5)	7480(9)	43(2)
C(18)	953(5)	7480(6)	2770(10)	55(3)	C(64)	7494(6)	6459(6)	8033(10)	58(3)
C(19)	788(5)	7052(6)	1801(9)	53(3)	C(65)	7603(6)	6870(6)	7073(10)	61(3)
C(20)	865(5)	6387(6)	2371(9)	52(3)	C(66)	7160(5)	6660(5)	5923(10)	50(3)
C(21)	−156(6)	4491(7)	394(10)	69(4)	C(67)	6632(6)	7928(5)	2350(11)	58(3)
C(22)	−815(7)	4841(8)	−40(12)	83(4)	C(68)	6399(7)	8496(6)	3112(12)	78(4)
C(23)	−405(5)	3571(5)	2827(12)	60(3)	C(69)	5315(6)	7219(6)	643(10)	61(3)
C(24)	53(7)	2958(7)	2910(14)	87(4)	C(70)	5490(8)	6823(7)	−527(11)	86(4)
C(25)	943(6)	3361(5)	7732(11)	58(3)	C(71)	4196(6)	4720(6)	715(10)	55(3)
C(26)	1106(7)	2753(6)	6953(14)	82(4)	C(72)	4492(7)	4783(8)	−527(11)	89(5)
C(27)	2292(5)	4123(5)	9218(9)	50(3)	C(73)	4768(5)	3417(5)	2168(9)	44(2)
C(28)	2090(7)	4499(7)	10354(10)	71(4)	C(74)	4201(5)	3193(5)	2947(12)	59(3)
C(29)	3162(6)	6723(6)	9056(10)	62(3)	C(75)	6345(7)	2958(6)	6905(13)	75(4)
C(30)	2933(8)	6634(7)	10360(11)	85(4)	C(76)	5647(7)	2736(7)	7042(14)	82(4)
C(31)	2394(5)	7982(5)	7533(10)	48(3)	C(77)	6810(5)	3922(6)	9310(9)	50(3)
C(32)	2915(6)	8255(6)	6732(10)	59(3)	C(78)	6225(6)	3982(7)	10094(9)	61(3)
C(33)	1013(6)	8242(6)	2724(12)	64(3)	C(79)	7903(8)	6455(7)	9428(12)	83(4)
C(34)	1753(6)	8466(7)	2598(14)	78(4)	C(80)	7515(9)	6801(8)	10250(17)	109(5)
C(35)	559(6)	7195(7)	390(10)	65(3)	C(81)	8151(6)	7435(6)	7119(13)	71(4)
C(36)	1139(10)	7183(11)	−311(16)	125(7)	C(82)	7866(11)	8049(8)	7432(17)	124(7)
C(37)	2304(6)	4827(6)	4212(10)	57(3)	C(83)	7601(5)	4997(5)	4948(10)	47(3)
C(38)	2950(6)	4653(8)	3831(11)	77(4)	C(84)	8191(5)	4797(6)	4447(10)	52(3)
C(39)	3349(6)	5176(11)	3455(11)	98(6)	C(85)	8209(5)	4851(5)	3168(10)	52(3)
C(40)	3133(6)	5813(10)	3473(12)	87(5)	C(86)	7629(5)	5088(5)	2368(10)	52(3)
C(41)	2514(5)	5928(7)	3869(9)	61(3)	C(87)	7057(5)	5270(5)	2896(9)	45(3)
C(42)	−206(5)	6075(5)	4910(10)	46(3)	C(88)	5192(5)	6507(5)	5668(9)	44(2)
C(43)	−842(6)	6167(6)	5362(11)	62(3)	C(89)	4584(5)	6715(6)	6037(10)	52(3)
C(44)	−834(5)	6098(6)	6672(11)	60(3)	C(90)	4112(5)	6259(6)	6376(10)	54(3)
C(45)	−226(5)	5965(6)	7465(11)	57(3)	C(91)	4269(5)	5605(6)	6326(9)	55(3)
C(46)	367(5)	5888(5)	6935(10)	49(3)	C(92)	4892(5)	5404(5)	5923(9)	42(2)

[a] Equivalent isotropic *U* defined as one-third of the trace of the orthogonalized $\mathbf{U}_{ij}$ tensor.

Discussion

Iron(II) bromide is readily inserted into a mixture of both isomeric forms of free base dioxoporphodimethene in tetrahydrofuran to yield high-spin, five-coordinate complexes. Like the parent free bases, the iron(III) isomers were not separable by chromatography, but successive fractional crystallizations did achieve samples which contained greater than 90% of the *trans* isomers. Pasteur separations could be carried out on these compounds, but crystal size and growth time made this a prohibitive option.

The presence of both isomers is easily detected by ^{1}H NMR spectroscopy because of the difference in molecular symmetry and relative intensity between the two compounds as seen for the Ni(II) complexes characterized previously.[9] The *trans* isomer, **10**, is more symmetric and generally present in about four times the quantity of the *cis* isomer, **11**. This combined with the large range of paramagnetic shifts inherent in these complexes allows for the clear assignment of resonances for **10** and **11**. The pattern of resonances of these isomers differ from other high-spin, five-coordinate porphyrin complexes such as XFe^{III}(OEP),[27] XFe^{III}(OEPOH)[13] and XFe^{III}(OEPOAc),[13] which have meso resonances that are shifted about 60−70 ppm upfield in chloroform-d_1 at room temperature. Compounds **10** and **11** have meso resonances which are shifted about 30−40 ppm downfield. This difference is likely the result of changes in the electronic structure of the dioxoporphodimethene ligands

(27) Goff, H. M. in *Iron Porphyrins Part I*; Lever, A. B. P., Gray, H. B., Eds.; Addison-Wesley: Massachusetts, Reading, MA, 1983; p 237.

Table 6. Bond Lengths (Å) and Angles (deg) for $(py)_2Fe^{II}(trans\text{-}OEPO_2)$

Bond Lengths (Å)

Molecule 1

Fe(1)−N(3)	1.927(7)	Fe(1)−N(2)	1.950(8)	C(4)−C(5)	1.448(14)	C(5)−C(6)	1.417(14)
Fe(1)−N(4)	1.957(8)	Fe(1)−N(5)	1.965(9)	C(6)−C(7)	1.412(13)	C(7)−C(8)	1.430(14)
Fe(1)−N(1)	1.974(8)	Fe(1)−N(6)	1.978(8)	C(8)−C(9)	1.348(13)	C(9)−C(10)	1.480(13)
O(1A)−C(1)	1.253(12)	O(2A)−C(11)	1.243(12)	C(10)−C(11)	1.403(13)	C(11)−C(12)	1.445(14)
O(1B)−C(6)	1.27(3)	O(2B)−C(16)	1.22(3)	C(12)−C(13)	1.424(14)	C(13)−C(14)	1.337(14)
N(1)−C(2)	1.349(12)	N(1)−C(5)	1.354(13)	C(14)−C(15)	1.401(13)	C(15)−C(16)	1.412(14)
N(2)−C(10)	1.352(12)	N(2)−C(7)	1.355(12)	C(16)−C(17)	1.405(14)	C(17)−C(18)	1.444(14)
N(3)−C(12)	1.348(11)	N(3)−C(15)	1.394(12)	C(18)−C(19)	1.33(2)	C(19)−C(20)	1.46(2)
N(4)−C(20)	1.375(12)	N(4)−C(17)	1.379(13)	C(37)−C(38)	1.41(2)	C(38)−C(39)	1.40(2)
N(5)−C(37)	1.338(14)	N(5)−C(41)	1.347(14)	C(39)−C(40)	1.34(2)	C(40)−C(41)	1.35(2)
N(6)−C(42)	1.285(11)	N(6)−C(46)	1.361(12)	C(42)−C(43)	1.400(14)	C(43)−C(44)	1.39(2)
C(1)−C(20)	1.44(2)	C(1)−C(2)	1.46(2)	C(44)−C(45)	1.33(2)	C(45)−C(46)	1.363(14)
C(2)−C(3)	1.42(2)	C(3)−C(4)	1.40(2)				

Molecule 2

Fe(2)−N(10)	1.947(7)	Fe(2)−N(8)	1.961(7)	C(51)−C(52)	1.410(14)	C(52)−C(53)	1.437(14)
Fe(2)−N(9)	1.961(8)	Fe(2)−N(7)	1.961(8)	C(53)−C(54)	1.445(13)	C(54)−C(55)	1.365(13)
Fe(2)−N(12)	1.984(7)	Fe(2)−N(11)	1.990(7)	C(55)−C(56)	1.416(13)	C(56)−C(57)	1.415(13)
O(3A)−C(52)	1.27(2)	O(4A)−C(62)	1.23(2)	C(57)−C(58)	1.361(13)	C(58)−C(59)	1.461(14)
O(3B)−C(57)	1.25(2)	O(4B)−C(47)	1.23(2)	C(59)−C(60)	1.373(14)	C(60)−C(61)	1.475(14)
N(7)−C(51)	1.351(11)	N(7)−C(48)	1.378(12)	C(61)−C(62)	1.447(13)	C(62)−C(63)	1.476(14)
N(8)−C(53)	1.348(11)	N(8)−C(56)	1.387(12)	C(63)−C(64)	1.410(14)	C(64)−C(65)	1.35(2)
N(9)−C(61)	1.354(11)	N(9)−C(58)	1.386(12)	C(65)−C(66)	1.414(14)	C(83)−C(84)	1.392(14)
N(10)−C(63)	1.360(12)	N(10)−C(66)	1.402(12)	C(84)−C(85)	1.360(14)	C(85)−C(86)	1.356(14)
N(11)−C(83)	1.346(12)	N(11)−C(87)	1.360(12)	C(86)−C(87)	1.367(14)	C(88)−C(89)	1.360(14)
N(12)−C(92)	1.325(12)	N(12)−C(88)	1.367(13)	C(89)−C(90)	1.38(2)	C(90)−C(91)	1.35(2)
C(47)−C(66)	1.396(14)	C(48)−C(49)	1.454(13)	C(91)−C(92)	1.396(14)		
C(49)−C(50)	1.324(14)	C(50)−C(51)	1.453(14)				

Bond Angles

Molecule 1

N(3)−Fe(1)−N(2)	89.6(3)	N(3)−Fe(1)−N(4)	91.0(3)	N(1)−C(5)−C(4)	109.1(8)	C(6)−C(5)−C(4)	123.1(9)
N(2)−Fe(1)−N(4)	178.9(3)	N(3)−Fe(1)−N(5)	91.2(3)	O(1B)−C(6)−C(7)	115.4(14)	O(1B)−C(6)−C(5)	121.2(14)
N(2)−Fe(1)−N(5)	91.4(3)	N(4)−Fe(1)−N(5)	89.5(4)	C(7)−C(6)−C(5)	121.7(9)	N(2)−C(7)−C(6)	122.4(8)
N(3)−Fe(1)−N(1)	179.4(3)	N(2)−Fe(1)−N(1)	90.1(3)	N(2)−C(7)−C(8)	113.7(8)	C(6)−C(7)−C(8)	123.8(9)
N(4)−Fe(1)−N(1)	89.2(3)	N(5)−Fe(1)−N(1)	89.4(3)	C(9)−C(8)−C(7)	105.5(9)	C(7)−C(8)−C(25)	127.7(9)
N(3)−Fe(1)−N(6)	89.3(3)	N(2)−Fe(1)−N(6)	87.8(3)	C(8)−C(9)−C(27)	128.0(9)	C(8)−C(9)−C(10)	105.8(9)
N(4)−Fe(1)−N(6)	91.2(3)	N(5)−Fe(1)−N(6)	179.1(4)	C(27)−C(9)−C(10)	126.1(8)	N(2)−C(10)−C(11)	122.6(8)
N(1)−Fe(1)−N(6)	90.1(3)	C(2)−N(1)−C(5)	108.7(8)	N(2)−C(10)−C(9)	111.0(8)	C(11)−C(10)−C(9)	125.4(8)
C(2)−N(1)−Fe(1)	127.9(7)	C(5)−N(1)−Fe(1)	123.4(6)	O(2A)−C(11)−C(10)	118.7(10)	O(2A)−C(11)−C(12)	118.0(10)
C(10)−N(2)−C(7)	104.0(8)	C(10)−N(2)−Fe(1)	127.6(6)	C(10)−C(11)−C(12)	123.1(8)	N(3)−C(12)−C(13)	110.9(9)
C(7)−N(2)−Fe(1)	128.4(6)	C(12)−N(3)−C(15)	104.0(8)	N(3)−C(12)−C(11)	121.9(8)	C(13)−C(12)−C(11)	127.1(8)
C(12)−N(3)−Fe(1)	128.2(7)	C(15)−N(3)−Fe(1)	127.8(6)	C(14)−C(13)−C(12)	107.5(8)	C(13)−C(14)−C(15)	106.4(9)
C(20)−N(4)−C(17)	104.7(8)	C(20)−N(4)−Fe(1)	128.6(8)	N(3)−C(15)−C(14)	111.2(8)	N(3)−C(15)−C(16)	122.7(9)
C(17)−N(4)−Fe(1)	126.5(6)	C(37)−N(5)−C(41)	116.5(10)	C(14)−C(15)−C(16)	124.7(9)	O(2B)−C(16)−C(17)	118(2)
C(37)−N(5)−Fe(1)	121.4(7)	C(41)−N(5)−Fe(1)	121.9(8)	O(2B)−C(16)−C(15)	117(2)	C(17)−C(16)−C(15)	124.2(9)
C(42)−N(6)−C(46)	116.5(8)	C(42)−N(6)−Fe(1)	121.4(6)	N(4)−C(17)−C(16)	124.4(9)	N(4)−C(17)−C(18)	110.4(9)
C(46)−N(6)−Fe(1)	121.9(6)	O(1A)−C(1)−C(20)	117.3(10)	C(16)−C(17)−C(18)	124.6(10)	C(19)−C(18)−C(17)	107.8(10)
O(1A)−C(1)−C(2)	121.0(10)	C(20)−C(1)−C(2)	121.6(8)	C(18)−C(19)−C(20)	106.3(8)	N(4)−C(20)−C(1)	122.7(9)
N(1)−C(2)−C(3)	110.1(9)	N(1)−C(2)−C(1)	123.8(8)	N(4)−C(20)−C(19)	110.7(10)	C(1)−C(20)−C(19)	126.1(8)
C(3)−C(2)−C(1)	125.6(9)	C(4)−C(3)−C(2)	106.2(9)	C(32)−C(31)−C(14)	110.4(9)		
C(3)−C(4)−C(5)	105.8(9)	N(1)−C(5)−C(6)	127.5(8)				

Molecule 2

N(10)−Fe(2)−N(8)	179.7(3)	N(10)−Fe(2)−N(9)	89.2(3)	C(48)−C(49)−C(67)	126.3(9)	C(49)−C(50)−C(51)	107.6(9)
N(8)−Fe(2)−N(9)	90.7(3)	N(10)−Fe(2)−N(7)	91.0(3)	N(7)−C(51)−C(52)	122.6(8)	N(7)−C(51)−C(50)	111.2(8)
N(8)−Fe(2)−N(7)	89.1(3)	N(9)−Fe(2)−N(7)	178.3(3)	C(52)−C(51)−C(50)	126.1(8)	O(3A)−C(52)−C(50)	119.5(11)
N(10)−Fe(2)−N(12)	90.5(3)	N(8)−Fe(2)−N(12)	89.3(3)	O(3A)−C(52)−C(53)	117.4(11)	C(51)−C(52)−C(53)	122.5(8)
N(9)−Fe(2)−N(12)	90.2(3)	N(7)−Fe(2)−N(12)	91.5(3)	N(8)−C(53)−C(52)	122.9(8)	N(8)−C(53)−C(54)	111.0(8)
N(10)−Fe(2)−N(11)	91.2(3)	N(8)−Fe(2)−N(11)	89.1(3)	C(52)−C(53)−C(54)	125.9(8)	C(55)−C(54)−C(53)	106.2(7)
N(9)−Fe(2)−N(11)	90.0(3)	N(7)−Fe(2)−N(11)	88.4(3)	C(54)−C(55)−C(56)	106.5(8)	N(8)−C(56)−C(55)	111.0(8)
N(12)−Fe(2)−N(11)	178.3(3)	C(51)−N(7)−C(48)	104.1(7)	N(8)−C(56)−C(57)	122.5(9)	C(55)−C(56)−C(57)	126.1(9)
C(51)−N(7)−Fe(2)	128.6(6)	C(48)−N(7)−Fe(2)	127.3(6)	O(3B)−C(57)−C(58)	120.3(11)	O(3B)−C(57)−C(56)	113.8(10)
C(53)−N(8)−C(56)	105.1(7)	C(53)−N(8)−Fe(2)	127.8(6)	C(58)−C(57)−C(56)	125.9(9)	C(57)−C(58)−N(9)	124.5(8)
C(56)−N(8)−Fe(2)	127.0(6)	C(61)−N(9)−C(58)	105.4(7)	C(57)−C(58)−C(59)	124.0(9)	N(9)−C(58)−C(59)	110.8(8)
C(61)−N(9)−Fe(2)	128.8(6)	C(58)−N(9)−Fe(2)	125.8(6)	C(60)−C(59)−C(58)	106.4(9)	C(59)−C(60)−C(61)	105.4(8)
C(63)−N(10)−C(66)	105.7(8)	C(63)−N(10)−Fe(2)	129.7(6)	N(9)−C(61)−C(62)	124.7(8)	N(9)−C(61)−C(60)	111.8(8)
C(66)−N(10)−Fe(2)	124.5(6)	C(83)−N(11)−C(87)	115.8(8)	C(62)−C(61)−C(60)	123.3(8)	O(4A)−C(62)−C(61)	121.4(11)
C(83)−N(11)−Fe(2)	120.7(7)	C(87)−N(11)−Fe(2)	123.4(6)	O(4A)−C(62)−C(63)	119.4(11)	C(61)−C(62)−C(63)	119.2(8)
C(92)−N(12)−C(88)	118.3(8)	C(92)−N(12)−Fe(2)	121.3(7)	N(10)−C(63)−C(64)	110.7(9)	N(10)−C(63)−C(62)	123.2(8)
C(88)−N(12)−Fe(2)	120.4(6)	O(4B)−C(47)−C(48)	115.0(11)	C(64)−C(63)−C(62)	125.4(9)	C(65)−C(64)−C(63)	106.9(9)
O(4B)−C(47)−C(66)	118.0(11)	C(48)−C(47)−C(66)	127.0(9)	C(64)−C(65)−C(66)	108.1(9)	C(47)−C(66)−N(10)	123.7(9)
C(47)−C(48)−N(7)	122.1(8)	C(47)−C(48)−C(49)	126.0(9)	C(47)−C(66)−C(65)	127.7(9)	N(10)−C(66)−C(65)	108.5(9)
N(7)−C(48)−C(49)	111.6(8)	C(50)−C(49)−C(48)	105.6(9)	C(82)−C(81)−C(65)	111.0(12)		

which are more highly oxidized than their porphyrin counterparts. The methylene and methyl protons exhibit a similar pattern of chemical shifts but have a greater magnitude than other related porphyrin systems.

Compound **10** is readily converted into an antiferromagnetically-coupled (μ-oxo)iron(III) dimer, **12**, by aqueous sodium hydroxide without detection of an iron(III) hydroxide monomeric intermediate, (OH)Fe^{III}(*trans*-OEPO$_2$). The properties of **12** are typical of those of other (μ-oxo)iron(III) porphyrin dimers.[21,28] The formation of additional isomeric μ-oxo dimers from a mixture containing **10** and **11** has been observed by ^{1}H NMR spectroscopy. Unfortunately, the small chemical shift range and broadness of the resonances prevented a rigorous identification of the other possible isomers. Addition of hydrochloric or hydrobromic acid cleaves **3** and regenerates the monomeric species.

The solid state structures of **10b** and **12** are completely ordered and corroborate the high-spin, five-coordinate nature of the species in solution. The *trans* keto assignment of oxygen atoms on the ligand is also clearly established. The dioxoporphodimethene macrocycle is domed in **10b** and roof-shaped in **12**. This is contrary to the slightly ruffled conformation adopted by the ClTl^{III}(*trans*-OEPO$_2$),[20] which contains a considerably larger metal ion. The differences in the monomers may be dictated by the solvent interactions and crystal packing noticeably present in these systems. Compound **12** contains the most acute Fe−O−Fe angle (165.4(2)°) reported for an untethered (μ-oxo)iron(III) porphyrin dimer. A distinctive trend in all of these *trans*-dioxoporphodimethene structures is an elongation of the macrocycle along an axis containing both oxidized meso carbons.

Both the monomers and the μ-oxo dimers autoreduce upon dissolution in pyridine to form diamagnetic bis(pyridine) iron(II) complexes. While the corresponding iron(III) octaethylporphyrin derivatives are not reduced by pyridine, a similar transformation has been observed for (Cl)$_2$Fe^{III}(OEOP).[5] The ease of reduction of these oxidized porphyrin ligands is likely a result of their increased Lewis acidity. The autoreduction of iron(III) octaethylporphyrin complexes has been reported for several other potential ligands such as piperidine, cynanide, *n*-hexanethiol, phosphine, and hydroxide ion.[29−36]

The solid state structure of **13** is confirmed by X-ray analysis and reveals slightly shortened Fe−N distances to axial and equatorial bound nitrogen atoms. This structure suffers from disordering of the oxygen atoms between the two possible *trans* configurations which is common for core modified porphyrins of this type.[5,8,9,24] Like (py)$_2$Ni^{II}(*trans*-OEPO$_2$),[9] the macrocycle is severely ruffled in the solid state, but ^{1}H NMR spectroscopy suggests a structure in solution which contains equivalent methylene protons. This is attributed to either rapid conformational interconversion of the macrocyclic ligand or a planar solution structure.

A comparison of the properties of ClFe^{III}(*trans*-OEPO$_2$) with those of ClFe^{III}(*trans*-OEPMe$_2$), **14**,[37] is warranted. Both

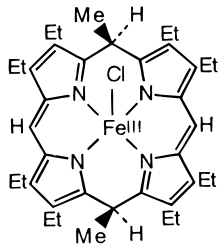

13, ClFe^{III}(*trans*-OEPMe$_2$)

macrocycles have modifications to a pair of trans meso positions and both complexes have high-spin ($S > {}^5/_2$) square pyramidal coordination for iron. Structurally there are important differences in the two macrocycles. For ClFe^{III}(*trans*-OEPMe$_2$) the macrocycle is folded along the line joining the two saturated meso carbon atoms and the out of plane displacements of the two types of meso carbon atoms are +0.56 and −0.59 Å, whereas for ClFe(*trans*-OEPO$_2$) the corresponding displacements are only 0.15 and 0.07 Å for the C=O carbons and +0.04 and −0.02 Å for the C−H carbons. The Fe−N and Fe−Cl distances (2.066(2) and 2.229(1) Å in ClFe^{III}(*trans*-OEPMe$_2$)) within the two structures are similar. Additionally there are similarities in the ^{1}H NMR spectra of ClFe^{III}(*trans*-OEPO$_2$) and ClFe^{III}(*trans*-OEPMe$_2$). The spectra of both complexes are dominated by downfield shifts of the methylene and meso proton resonances. For ClFe^{III}(*trans*-OEPMe$_2$) the methylene resonances occur as a doublet at 78 and 69 ppm and a second doublet at 34 and 41 ppm and the meso proton resonance appears at 11 ppm at 293 K. In both cases the downfield bias on these chemical shifts is likely to result from the presence of spin transfer through the σ bond system.

These structural studies set the stage for detection of iron complexes of the dioxoporphodimethenes during reactions that lead to heme peripheral modification and degradation.

Experimental Section

Preparation of Compounds. A 4:1 mixture of the dioxo ligands **8** and **9** was obtained as described previously.[9,12]

XFe^{III}(*trans*-OEPO$_2$), 10, XFe^{III}(*cis*-OEPO$_2$), 1, (X: a = Br, b = Cl). A 67 mg sample of dioxoporphodimethene free bases **8** and **9** was brought to a slow boil in 80 mL of reagent grade tetrahydrofuran. To this yellow-brown solution was added 283 mg of iron(II)bromide hexahydrate with 20 mL of tetrahydrofuran. The red-brown solution was slowly boiled until the volume was reduced to about 20 mL. The remaining solvent was removed under vacuum. The solids were redissolved in 100 mL of dichloromethane, washed twice with 100 mL volumes of distilled water, and finally washed with 100 mL of a 5% (v/v) hydrobromic (X = Br$^-$) or hydrochloric (X = Cl$^-$) acid solution. The organic layer was collected and dried over sodium sulfate, and the solvent was removed under vacuum to give 52 mg (63% yield) of product as a green solid.

XFe^{III}(*trans*-OEPO$_2$), 10a,b. ^{1}H NMR (X = Br) ($CDCl_3$, 25 °C), δ, ppm: 31.35 (2 H, s, meso); 54.96, 57.02, 73.91, 74.78 (16 H, 4 s, methylene); 7.12, 7.96 (24 H, 2 s, methyl). ^{1}H NMR (X = Cl$^-$) ($CDCl_3$, 25 °C), δ, ppm: 27.72 (2 H, s, meso); 52.92, 53.59, 70.13, 71.16 (16 H, 4 s, methylene); 6.00, 7.03 (24 H, 2 s, methyl). UV/vis (X = Cl$^-$, in CH_2Cl_2), λ_{max}, nm (ϵ, M^{-1} cm^{-1}): 338 (66 000) 423 (118 500) 585 (20 500) 933 (2800). UV/vis (X = Cl$^-$, in pyridine) 424 (18 300) 562 (5100). IR (X = Cl$^-$, solid): ν(C=O), 1603 cm^{-1}.

XFe^{III}(*cis*-OEPO$_2$), 11a. ^{1}H NMR (X = Br$^-$) ($CDCl_3$, 25 °C), δ, ppm: 40.11 (2 H, s, meso); 41.37, 42.92, 60.67, 60.90, 68.82, 74.42, 85.36, 89.17 (16 H, 8 s, methylene); 6.34−8.78 (24 H, 4 s, methyl). ^{1}H NMR (X = Cl$^-$) ($CDCl_3$, 25 °C), δ, ppm: 35.45 (2 H, s, meso); 40.31, 40.87, 57.23, 58.35, 64.63, 70.50, 82.86, 83.80 (16 H, 8 s, methylene); 5.18−7.89 (24 H, 4s, methyl).

{Fe^{III}(*trans*-OEPO$_2$)}$_2$O, 12. A 30 mg sample of **10** and **11** was dissolved in 50 mL of dichloromethane and washed twice with 50 mL portions of a 0.5 M aqueous sodium hydroxide solution. The organic

(28) Scheer, H.; Katz, J. J. In *Porphyrins and Metalloporphyrins*; Smith, K. M., Ed.; Elsevier: New York, 1975; p 399.
(29) Castro, C. E.; Jamin, M.; Yokoyama, W.; Wade, R. *J. Am. Chem. Soc.* **1986**, *108*, 4179.
(30) Modi, S.; Shedbalkar, V. P.; Behere, D. V. *Inorg. Chim. Acta* **1990**, *173*, 9.
(31) Del Gaudio, J.; La Mar, G. N. *J. Am. Chem. Soc.* **1978**, *100*, 1112.
(32) Epstein, L. M.; Straub, D. K.; Maricondi, C. *Inorg. Chem.* **1967**, *6*, 1720.
(33) Del Gaudio, J.; La Mar, G. N. *J. Am. Chem. Soc.* **1976**, *98*, 3014.
(34) Del Gaudio, J.; La Mar, G. N. *Adv. Chem. Ser.*, **1977**, *162*, 207.
(35) Srivasta, G. S.; Sawyer, D. T. *Inorg. Chem.* **1985**, *24*, 1732.
(36) Shin, K.; Kramer, S. K.; Goff, H. M. *Inorg. Chem.*, **1987**, *26*, 4103.
(37) Botulinski, A.; Buchler, J. W.; Lee, Y. J.; Scheidt, W. R.; Wicholas, M. *Inorg. Chem.* **1988**, *27*, 927.

layer was collected and dried over sodium sulfate, and the solvent was removed under vacuum to give 25 mg (83% yield) of dimers as a red-green solid. The dimer can also be prepared by chromatography on neutral alumina. A 30 mg sample of **10** and **11** run on a 10 cm long × 2.5 cm diameter column with dichloromethane eluant yields 77% (23 mg) of μ-oxo dimers as the first green band. Successive fractional crystallizations from dichloromethane−ethanol solutions gave samples which contained >90% isomeric purity of **13**.

^{1}H NMR ($CDCl_3$, 25 °C), δ, ppm: 6.60 (4 H, s, meso); 4.24, 4.81, 5.40, 6.29 (32 H, 4 s, methylene); 1.00, 1.16 (48 H, 2 s, methyl). UV/vis (in CH_2Cl_2), λ_{max}, nm (ϵ, M^{-1} cm^{-1}): 330 (67 600) 398 (48 300) 437 (53 400) 584 (21 100) 887 (2000). UV/vis (in pyridine), λ_{max}, nm (ϵ, M^{-1} cm^{-1}):: 436 (48900) 583 (19900) 882 (1600). IR (solid): ν(C═O), 1590 cm^{-1}.

(py)$_2$Fe^{II}(*trans*-OEPO$_2$), 13. ^{1}H NMR samples of the iron(III) monomers and dimers in pyridine-d_5 were heated to 65 °C for 1 day to convert the samples to their bis(pyridyl)iron(II) analogs. The compounds are air stable in pyridine solution for weeks. Pyridine solutions of the iron(III) complexes rapidly form the iron(II) complexes in the presence of ascorbic acid. A 15.0 mg sample of **12** (>90% trans isomer) was dissolved in 20 mL of pyridine and briefly stirred with a slight excess of ascorbic acid until the solution turned red. The solution was then diluted with 40 mL of dichloromethane and washed with 25 mL of water. The organic layer was separated and vacuum dried to give 12.3 mg of red solid (66% yield).

^{1}H NMR (pyridine-d_5 , 25 °C), δ, ppm: 6.91 (2 H, s, meso); 2.58, 3.08 (16 H, 2 q, methylene); 1.14, 1.36 (24 H, 2 t, methyl). UV/vis (in pyridine), λ_{max}, nm (ϵ, M^{-1} cm^{-1}): 373 (11 000) 425 (12 400) 447 (12 300) 504 (sh) (6600) 582 (sh) (3900) 712 (sh) (1100). IR (solid): ν(C═O), 1592 cm^{-1}.

Instrumentation. ^{1}H NMR spectra were recorded on a General Electric QE 300 Fourier transform spectrometer operating in the quadrature mode (^{1}H frequency is 300 MHz). The spectra were collected over a 30-kHz bandwidth with 16k data points and a 5 μs 45° pulse. The signal to noise ratio was improved by apodization of the free induction decay. Electronic spectra were obtained through the use of a Hitachi U-2000 spectrophotometer. Infrared spectra were collected on an IBM IR/32 spectrometer. EPR spectra were obtained using a Bruker spectrometer. The magnetic moments were measured by the Evans technique.[38]

X-ray Data Collection. **{ClFe^{III}(*trans*-OEPO$_2$)}·1.5C$_6$H$_6$, 10b.** Dark red plates were obtained by slow diffusion of *n*-hexane into a benzene solution of the compound. A suitable crystal was coated with a light hydrocarbon oil and mounted in the 123 K dinitrogen stream of a Siemens P4/RA diffractometer which was equipped with a locally modified LT-2 low temperature device. Intensity data were collected with nickel-filtered Cu Kα radiation from a Siemens rotating anode X-ray generator that operated at 15 kW. Crystal data are given in Table 7. No decay (<2%) in the intensities of two standard reflections was observed during data collection. The data were corrected for Lorentz and polarization effects.

{Fe^{III}(*trans*-OEPO$_2$)}$_2$O, 12. Dark purple blocks were obtained by slow diffusion of iso-octane into a dichloromethane solution of the compound. A suitable crystal was coated with a light hydrocarbon oil and mounted on a Siemens R3m/V diffractometer. The crystals underwent a catastrophic phase change upon cooling in a liquid nitrogen stream. Thus, the data set was collected at room temperature (294 K). Intensity data were collected with Mo Kα radiation using a highly oriented graphite crystal monochromator. Two check reflections showed only random (<2%) variation in intensity during data collection. The data were corrected for Lorentz and polarization effects. Crystal data are given in Table 7.

{(py)$_2$Fe^{II}(*trans*-OEPO$_2$)}, 13. Slow evaporation of a pyridine/water solution gave dark plates suitable for diffraction. Data were obtained at 130 K as described above for {ClFe^{III}(*trans*-OEPO$_2$)}·1.5C$_6$H$_6$, **10b**.

Structure Solution and Refinement. Calculations were performed with SHELXTL Plus (Sheldrick, Siemens, 1990) and SHELXL-93 (Sheldrick, 1993). Scattering factors and corrections for anomalous dispersion were taken from a standard source.[39] The solution for each compound was accomplished by a Patterson function with subsequent cycles of least-squares refinement and calculation of difference Fourier maps. Hydrogen atoms were included with the use of a riding model. An absorption correction was applied.[40]

Table 7. Crystal Structure Data

	ClFe^{III}(*trans*-OEPO$_2$)	[Fe^{III}(*trans*-OEPO$_2$)]$_2$O	(py)$_2$Fe^{II}(*trans*-OEPO$_2$)
formula	$C_{45}H_{51}ClFeN_4O_2$	$C_{36}H_{42}FeN_4O_{2.5}$	$C_{92}H_{100}Fe_2N_{12}O_4$
fw	771.2	626.6	1549.5
space group	$P2_1/c$, monoclinic	$C2/c$, monoclinic	$P2_1$, monoclinic
a (Å)	13.766(3)	23.541(8)	19.177(4)
b (Å)	19.075(3)	15.392(5)	20.039(4)
c (Å)	15.217(3)	18.686(8)	10.547(2)
α (deg)	90	90	90
β (deg)	99.87(2)	90.09(3)	100.36(3)
γ (deg)	90	90	90
V (Å^3)	3936.4(12)	6770(3)	3936.4(12)
T (K)	123	294	130
Z	4	8	2
d_{calc} (Mg/m^3)	1,301	1.229	1.291
radiation (Å)	λ(Cu Kα) = 1.541 78	λ(Mo Kα) = 0.710 73	λ(Cu Kα) = 1.541 78
μ (mm^{-1})	4.026	0.483	3.392
R^a	0.0624	0.0484	0.0684
$R_w{}^b$ or wR2^c	0.0596^b	0.0527^b	0.1763^c

^{a} $R = \sum||F_o| - |F_c||/\sum|F_o|$. ^{b} $R_w = \sum||F_o| - |F_c||w^{1/2}/\sum|F_o|w^{1/2}$. ^{c} wR2 = $[\sum[w(F_o^2 - F_c^2)^2]/\sum[w(F_o^2]]^{1/2}$.

For {ClFe^{III}(*trans*-OEPO$_2$)}·1.5C$_6$H$_6$, **10b**, the Fe and Cl atoms were refined with anisotropic thermal parameters. The largest peak in the difference map was +0.95 e Å^{-3}, and the largest hole was −0.48 e Å^{-3}.

For {Fe^{III}(*trans*-OEPO$_2$)}$_2$O, **12**, all non-hydrogen atoms were refined with anisotropic thermal parameters. The largest peak in the difference map was +0.54 e Å^{-3}, and the largest hole was −0.36 e Å^{-3}.

For {(py)$_2$Fe^{II}(*trans*-OEPO$_2$)}, **13**, all non-hydrogen atoms were refined with anisotropic thermal parameters. The compound crystallizes as a racemic twin, and refinement was carried out using the TWIN subroutine of SHELXL-93. The indications for twinning and method of refinement were analogous to those employed in the analysis of the structure of {(py)$_2$Co^{III}(OEPO)}, which is isostructural with {(py)$_2$Fe^{II}(*trans*-OEPO$_2$)}.[41] The largest peak in the difference map was +1.475 e Å^{-3}, and the largest hole was −0.961 e Å^{-3}. There are two molecules in the unit cell and each displays some disorder. Two alternate sets of positions, A and B, for the *trans* placement of the oxygen atoms at the meso positions were found. Thus the thermal parameters for {O(1A), O(2A)} and {O(1B), O(2B)} were tied together and their occupancies required to sum to 1.0 for molecule 1. Likewise, for molecule 2, {O(3A), O(4A)} and {O(3B), O(4B)} were treated in the same manner. Refinement resulted in oxygen atom occupancies of (71/29) and (50/50) for sets A and B of the two distinct molecules, respectively.

Acknowledgment. We thank the National Institutes of Health (Grant GM26226) for support.

Supporting Information Available: Details of data collection and structure refinement, tables of atomic coordinates, bond distances and angles, anisotropic thermal parameters, and hydrogen atom positions for **10b**, **12**, and **13** and a drawing showed the unit cell of **10b** (36 pages). Ordering information is given on any current masthead page.

IC960423V

(38) Evans, D. F. *J. Chem. Soc.* **1959**, 2003.

(39) *(39) International Tables for X-ray Crystallography*; D. Reidel Publishing Co.: Boston, MA, 1992; Vol. C.

(40) Parkin, S. R.; Moezzi, B.; Hope, H. *J. Appl. Crystallogr.* **1995**, *28*, 53.

(41) Balch, A. L.; Mazzanti, M.; Olmstead, M. M. *Inorg. Chem.* **1993**, *32*, 4737.